JCB

Protease signaling regulates apical cell extrusion, cell contacts, and proliferation in epithelia

Antonino Schepis,[1] Adrian Barker,[1] Yoga Srinivasan,[1] Eaman Balouch,[1] Yaowu Zheng,[1] Ian Lam,[1] Hilary Clay,[1] Chung-Der Hsiao,[2] and Shaun R. Coughlin[1]

[1]Cardiovascular Research Institute, University of California, San Francisco, San Francisco, CA
[2]Department of Bioscience Technology, Chung Yuan Christian University, Chung-Li, Taiwan

Mechanisms that sense and regulate epithelial morphogenesis, integrity, and homeostasis are incompletely understood. Protease-activated receptor 2 (Par2), the Par2-activating membrane-tethered protease matriptase, and its inhibitor, hepatocyte activator inhibitor 1 (Hai1), are coexpressed in most epithelia and may make up a local signaling system that regulates epithelial behavior. We explored the role of Par2b in matriptase-dependent skin abnormalities in Hai1a-deficient zebrafish embryos. We show an unexpected role for Par2b in regulation of epithelial apical cell extrusion, roles in regulating proliferation that were opposite in distinct but adjacent epithelial monolayers, and roles in regulating cell–cell junctions, mobility, survival, and expression of genes involved in tissue remodeling and inflammation. The epidermal growth factor receptor Erbb2 and matrix metalloproteinases, the latter induced by Par2b, may contribute to some matriptase- and Par2b-dependent phenotypes and be permissive for others. Our results suggest that local protease-activated receptor signaling can coordinate cell behaviors known to contribute to epithelial morphogenesis and homeostasis.

Introduction

Protease-activated receptors (PARs) are G protein–coupled receptors that mediate cellular responses to extracellular proteases (Vu et al., 1991a). Site-specific cleavage of the N-terminal ectodomain of these receptors serves to uncover a tethered peptide ligand, which binds to the receptor's heptahelical bundle to effect transmembrane signaling and G protein activation (Vu et al., 1991a,b). Among the four PARs found in mammals, PAR1, PAR3 and PAR4 mediate cellular responses to the coagulation protease thrombin. Genetic studies in mice and pharmacological studies in humans suggest that signaling via these receptors helps orchestrate physiological responses to tissue injury including hemostasis and perhaps inflammation and repair (Coughlin, 2000, 2005). The identity of the physiological activators of PAR2 and its roles in vivo are less explored.

Studies in cell culture and mice suggest that Par2 together with the protease matriptase and its inhibitors Hai1 and Hai2, all integral membrane proteins, may make up a local signaling system that regulates epithelial behavior (Takeuchi et al., 2000; Camerer et al., 2010; Szabo and Bugge, 2011; Sales et al., 2015b). Matriptase, gene symbol *St14*, is a type 2 integral membrane protein that displays a trypsin-like serine protease domain extracellularly. Subnanomolar concentrations of soluble matriptase protease domain can cleave and activate Par2 in cell culture (Takeuchi et al., 2000; Camerer et al., 2010); heterologous coexpression of full-length matriptase with Par2 can also promote Par2 cleavage (Camerer et al., 2010). Par2, matriptase, Hai1, and Hai2 are naturally coexpressed in most epithelial tissues (Takeuchi et al., 2000; Camerer et al., 2010; Szabo and Bugge, 2011; Sales et al., 2015b). In the mouse embryo, Par2 is expressed in ectodermal epithelium at the time and place of neural tube closure. Loss of Par2 function in certain genetic backgrounds can impair this process, as can loss of Hai2 function (Szabo et al., 2009; Camerer et al., 2010). Conditional knockout of the matriptase gene in the epithelial cells of mouse intestine or skin leads to defective barrier function in these tissues. Intestinal knockout leads to gut inflammation and skin knockout to perinatal death from desiccation (List et al., 2002, 2009). Overexpression of matriptase or the matriptase activator prostasin in mouse skin leads to hyperplasia, inflammation, ichthyosis, and pruritus, and these phenotypes are mimicked by Par2 overexpression and prevented by Par2 deficiency (Steinhoff et al., 2003; Frateschi et al., 2011; Sales et al., 2015a,b). Although matriptase has multiple substrates (Takeuchi et al., 2000; Antalis et al., 2011) and Par2 can be activated by other trypsin-like proteases (Nystedt et al., 1994; Corvera et al., 1997; Camerer et al., 2000; Zhao et al., 2014), these and other data suggest that matriptase and Par2 may comprise a local signaling system that contributes to the formation and function of epithelial tissues (Camerer et al., 2010; Szabo et al., 2014; Le Gall et al., 2016; Fig. 1 A). However, the precise cellular behaviors regulated by this system and its physiological roles remain to be fully illuminated.

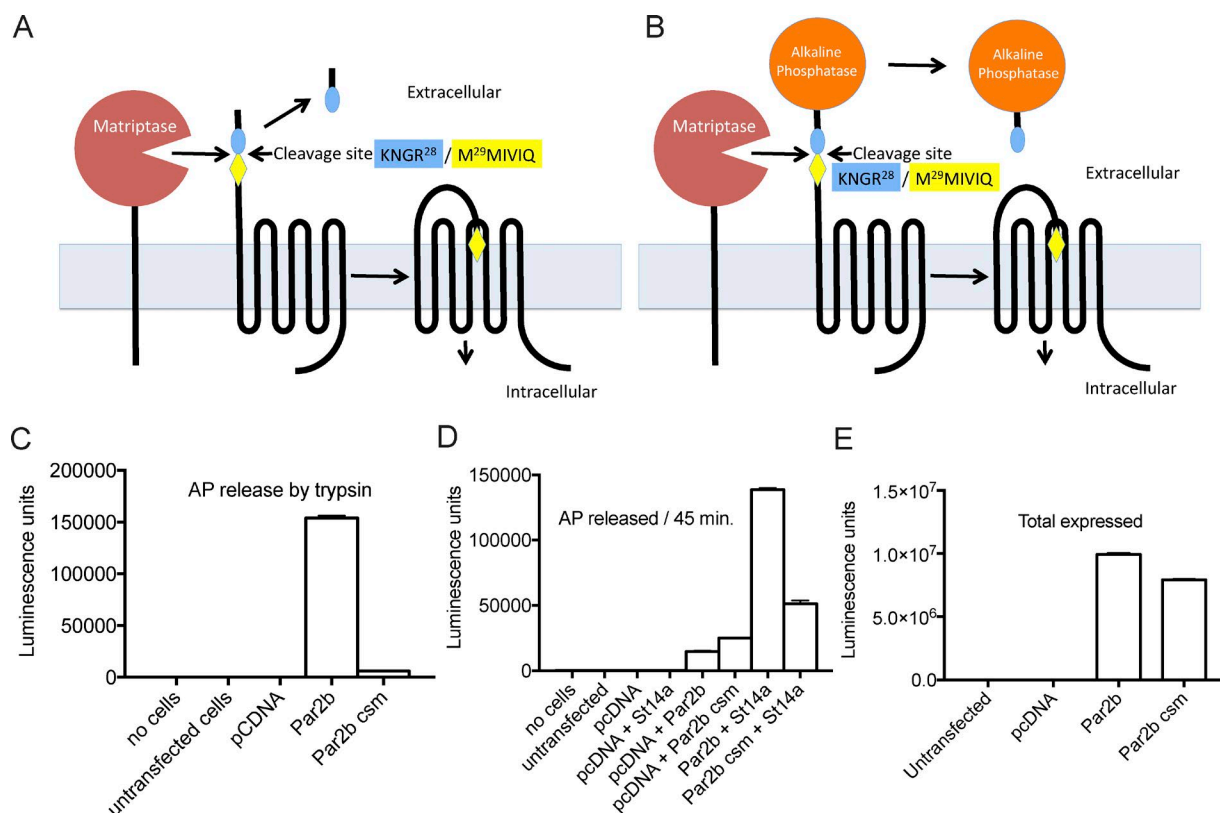Correspondence to Shaun R. Coughlin: shaun.coughlin@ucsf.edu

Figure 1. **Zebrafish matriptase cleaves Par2b. (A)** Proposed Par2b activation mechanism. Cleavage at R28/M29 unmasks tethered peptide ligand. **(B)** AP-Par2b cleavage reporter. Cleavage releases AP to conditioned medium. **(C–E)** HEK293 cells were cotransfected with empty pcDNA3.1 or the same vector directing expression of the Par2b cleavage reporter AP-Par2b, AP-Par2b carrying a R28A/M29P mutation to ablate the predicted activating cleavage site (AP-Par2b csm), or zebrafish matriptase (St14a). AP activity released into the conditioned medium was measured luminometrically. **(C)** AP released by trypsin treatment (4 nM for 10 min) to measure releasable AP. **(D)** AP released during a 45-min incubation to assess the effect of matriptase (St14a) expression. **(E)** AP activity in detergent extracts of cells expressing AP-Par2b or AP-Par2bmut was measured as an index of total expression of the reporter constructs. Data shown are mean ± SEM of three biological replicates, with AP activity expressed as arbitrary luminescence units. This experiment was done three times with similar results.

Epithelial growth and remodeling, epithelial-to-mesenchymal transformation, and signaling from epithelium to other cells play central roles in morphogenesis and organogenesis during embryonic development. Epithelial barriers between tissues and between an organism and its environment play key roles in adult physiology and homeostasis by regulating the movement and delivery of molecules between compartments (Marchiando et al., 2010). To support these vital functions, epithelia must regulate cell junctions, polarity, shape, size, movement, density, and number and jettison crowded or damaged cells—all without losing barrier function (Ragkousi and Gibson, 2014; Gudipaty and Rosenblatt, 2017). Given the evidence that Par2 activation by matriptase can contribute to development and homeostasis of epithelial tissues, we sought a system in which the roles of matriptase and Par2 activation in an epithelium could be explored in detail.

The zebrafish system offers genetic tractability and external development of large numbers of optically transparent embryos amenable to video microscopy. The skin of the early zebrafish embryo is a simple bilayer epithelium composed of an outer periderm layer and an inner basal layer (Le Guellec et al., 2004). Periderm keratinocytes adhere tightly to each other and form tight junctions to create a strong epithelial barrier (Kiener et al., 2008; Kwong and Perry, 2013). Basal layer keratinocytes adhere to each other and to the periderm through E-cadherin, the extracellular component of the adherens junctions, and

hemidesmosomes (Slanchev et al., 2009; Sonawane et al., 2009). Deficiency of the matriptase inhibitor Hai1a (also known as Spint1a) in zebrafish embryos causes abnormal skin development characterized by accumulation of cell clusters on the skin surface, altered cell–cell contacts, leukocyte infiltration, and other abnormalities (Carney et al., 2007; Mathias et al., 2007). Deficiency of the matriptase homologue St14a rescues these phenotypes, suggesting that they are mediated by increased matriptase activity associated with loss of its inhibition by Hai1a (Carney et al., 2007; Mathias et al., 2007). The availability of a matriptase-dependent epithelial phenotype in zebrafish embryos provided an opportunity to search for and characterize roles of matriptase-driven Par2 signaling in a vertebrate epithelium.

Results

Par2b is coexpressed with matriptase and Hai1a in the skin of the zebrafish embryo

To determine whether a local matriptase-Hai1-Par2 system might operate in zebrafish embryonic epidermis, we first asked whether its components are coexpressed in the cell types that make up this tissue. We isolated periderm or basal layer cells by FACS from embryos collected at 24 h postfertilization (hpf) using zebrafish lines carrying a fluorescent marker for

periderm (*Tg (krt4:nlsEGFP)^{cy34}*) or basal layer (*TgBAC (ΔNp63:Gal4FF)^{la213};Tg (uas:LifeActGFP)^{mu271}*). These lines are hereafter called periderm-nuclear-EGFP and basal-layer-LifeActGFP, respectively. Compared with RNA from whole embryos, RNA from the sorted periderm cell preparation was enriched ∼17-fold for the periderm markers *krt5* and *krt4* but showed no enrichment for the basal marker *p63*. RNA from the sorted basal layer cell preparation was enriched approximately fivefold for *p63* but showed no enrichment for *krt4* (Table S1). Thus, the sorted cell populations showed enrichment for the expected markers.

mRNAs encoding the Hai1 zebrafish homologue Hai1a, the matriptase homologue St14a, and the Par2 homologue Par2b (also known as F2rl1.2) were readily detected in both the periderm and basal layer preparations and enriched compared with whole embryo. The level of *hai1a*, *st14a*, and *par2b* mRNA in periderm preparations was ∼9-, ∼9-, and ∼16-fold enriched, respectively, compared with whole embryo. In basal layer, *hai1a*, *st14a*, and *par2b* mRNA were enriched ∼10-, ∼4-, and ∼8-fold, respectively (Table S1). These results suggest that matriptase gene *st14a* and the Hai1 gene *hai1a* are coexpressed with *par2b* in both the periderm and the basal layer of zebrafish embryo skin. Previous in situ hybridization studies indicated expression of *hai1a* in the skin of the zebrafish embryo (Carney et al., 2007).

Zebrafish matriptase can cleave zebrafish Par2b at its activation site

The Par2b N-terminal exodomain contains the amino acid sequence KNGR^{28}/M^{29}. Studies of mammalian matriptase substrate specificity (Takeuchi et al., 2000) suggest that matriptase should cleave this sequence at the R^{28}/M^{29} peptide bond (Fig. 1 A). To determine whether zebrafish matriptase can indeed cleave zebrafish Par2b like the cognate mammalian proteins, we generated the cleavage reporter AP-Par2b in which secreted AP is joined to the N-terminal ectodomain of Par2b. Cleavage of AP-Par2b at R^{28}/M^{29}, its predicted activating cleavage site, should release AP into the culture medium (Fig. 1 B; Ludeman et al., 2004; Camerer et al., 2010). Trypsin efficiently cleaves mammalian PAR2 at its activating cleavage site (Nystedt et al., 1994; Camerer et al., 2010). As a positive control, we first determined whether AP-Par2b is cleaved by exogenously added trypsin. Trypsin treatment of AP-Par2b–expressing HEK293 cells released ∼150,000 arbitrary units (AU) AP to conditioned medium (Fig. 1 C). No such increase was seen with trypsin treatment of untransfected cells or cells expressing an AP-Par2b R^{28}A/M^{29}P mutant in which the predicted activating cleavage site was ablated (Fig. 1 C). These results suggest that trypsin can cleave AP-Par2b at the predicted KNGR^{28}/M^{29} activation site and are consistent with the observation that trypsin triggers Par2b internalization (Xu et al., 2011) as well as the notion that, like mammalian Par2, zebrafish Par2b can sense trypsin-like proteases.

Cells expressing AP-Par2b alone released ∼15,000 AU AP during a 45-min sampling period. Coexpression of zebrafish matriptase with AP-Par2b was associated with release of ∼139,000 AU AP during a 45-min sampling period, a net increase of ∼124,000 AU and ninefold that released in the absence of matriptase expression (Fig. 1 D). Cells expressing the cleavage site mutant AP-Par2b R^{28}A/M^{29}P alone released ∼25,000 AU of AP during the sampling period. Coexpression of zebrafish matriptase with the cleavage mutant was associated

with release of ∼51,000 AU AP, a net increase of ∼26,000 AU—only twofold that released in the absence of matriptase and ∼20% of the increase in AP release seen when wild-type AP-Par2b was expressed with matriptase (Fig. 1 D). Total expression of AP-Par2b and AP-Par2b R^{28}A/M^{29}P was similar in these experiments (Fig. 1 E). At face value, these data suggest that, during the sampling period, ∼80% of AP release associated with coexpression of zebrafish matriptase with AP-Par2b was caused by AP-Par2b cleavage at the KNGR^{28}/M^{29} site, with ∼20% of cleavage occurring at another site. Other potentially matriptase-sensitive sites include K^{25}/N^{26} or R^{47}/E^{48}. Although we cannot exclude an indirect action of matriptase (e.g., by activating an intermediate protease), these results suggested that the zebrafish matriptase can cleave zebrafish Par2b at its predicted activating cleavage site and hence serve as a Par2b activator. Subsequent genetic experiments described in the following paragraphs are consistent with this notion.

Abnormal skin morphology in *hai1a* morphant embryos is par2b dependent

As noted in the Introduction, loss of function for the matriptase inhibitor Hai1a by mutation or morpholino (MO) knockdown is associated with matriptase-dependent skin abnormalities characterized by clusters of cells on the surface of the skin of zebrafish embryos (Carney et al., 2007; Mathias et al., 2007; Fig. 2, A, B, and E). The results we have described suggest the possibility that matriptase-driven Par2b activity associated with removal of matriptase inhibition might contribute to the *hai1a* phenotype. To test this hypothesis, we removed matriptase inhibition by using *hai1a* MOs and replicated key findings with *hai1a* mutants. Mutant *hai1a* phenotypes were sometimes more severe than morphants but were otherwise indistinguishable. Conversely, to ensure new findings regarding the role of Par2b would not be confounded by off-target effects, we removed Par2b activity using a *par2b* mutant generated with transcription activator-like effector nucleases (TALENs; see Materials and Methods and supplemental data file) and replicated selected phenotypes using *par2b* morphants.

We first examined the effect of matriptase (St14a) or Par2b deficiency on the presence of cell clusters on the skin of *hai1a* morphants (Fig. 2, A–E). No skin cell clusters were detected in uninjected wild-type or *par2b* mutant embryos that did not receive *hai1a* MO. 95% of embryos injected with *hai1a* MO showed clusters, but only 11% of *hai1a* morphants coinjected with *st14a* MO, 9% of *par2b$^{-/-}$ hai1a* morphants, and 21% of embryos coinjected with *hai1a* and *par2b* MOs showed clusters (Fig. 2 E). The observation that knockdown of *st14a* expression prevents the appearance of cell clusters in *hai1a* morphants is consistent with prior work and with the model that increased matriptase activity contributes to this phenotype (Carney et al., 2007; Mathias et al., 2007). The observation that *par2b* mutation or MO knockdown also prevents the appearance of cell clusters on the skin of *hai1a* morphants is consistent with the hypothesis that Par2b activation by matriptase contributes to the *hai1a* phenotype.

In addition to cell clusters on the skin surface (Fig. 2 B), *hai1a* mutant and morphant zebrafish embryos have a variety of abnormalities in basal layer keratinocytes, including loss of cell–cell contacts and increased motility and proliferation (Carney et al., 2007). Periderm has not been studied in similar detail in this model. Hai1a-deficient embryos also exhibit increased expression of inflammation markers as well as
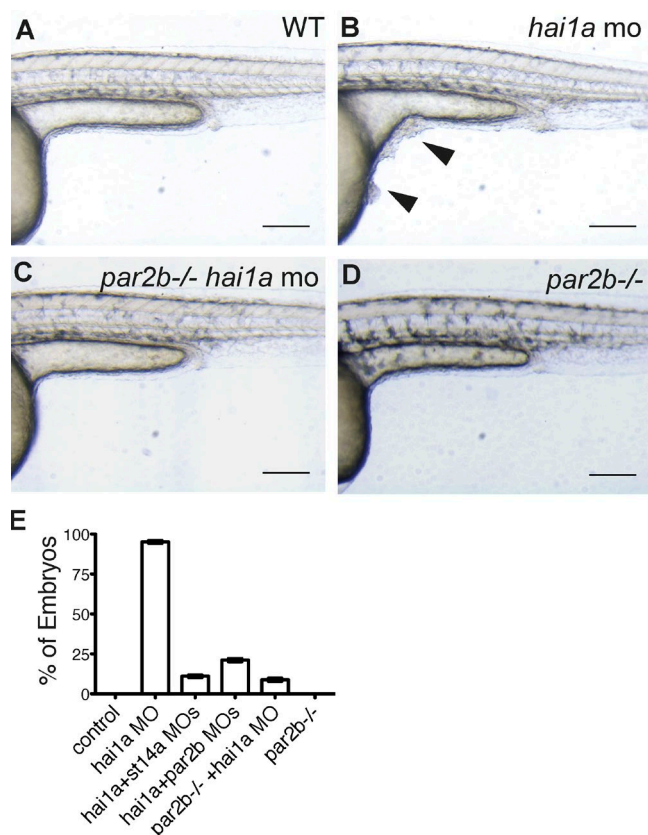
Figure 2. **Par2b deficiency prevents grossly abnormal skin morphology in *hai1a* morphants.** **(A–D)** Wild-type or *par2b*−/− embryos were injected with the indicated MOs and imaged at 30 hpf. Images of control (A), *hai1a* morphant (B), *par2b*−/−:*hai1a* morphant (C), and *par2b*−/− embryos (D) are shown. Note the presence of cell clusters on *hai1a* morphants (B, arrowheads) and their absence on controls and Par2b-deficient *hai1a* morphants. Bar, 200 µm. **(E)** Percentage of embryos with cell clusters. 100 or more embryos were analyzed for each condition; mean ± SEM for three independent experiments is shown. Statistical analysis was performed using one-way ANOVA and Bonferroni posttest. The *hai1a* morphant was different from all other groups (P < 0.0001).

leukocyte infiltration of tissues (Mathias et al., 2007; LeBert et al., 2015). Thus, Hai1a-deficient zebrafish embryos provided an opportunity to probe the role of Par2b in a variety of epithelial functions in the basal layer and in inflammatory responses and to uncover new roles in periderm.

Periderm keratinocytes undergo apical extrusion in *hai1a* morphants in a matriptase- and par2b-dependent manner

Toward understanding the nature of the cell clusters in *hai1a* morphants and the effect of Par2b deficiency, we first performed time-lapse vital microscopy using a Tg (krt4:Sce.Abp140 -Venus)^{cy22} line, hereafter called periderm-LifeActGFP, which expresses a fluorescent marker for filamentous actin (F-actin) in periderm keratinocytes. Because abnormal skin morphology in *hai1a* mutants was most frequent and most obvious over the ventral yolk sac and at the junction of the yolk sac and trunk (Fig. 2 B), this region (Fig. S1) was imaged from 28 to 46 hpf in 10 embryos for each condition.

In control periderm-LifeActGFP embryos, little change in the arrangement of cells or F-actin distribution was noted over the imaging period (Video 1). Strikingly, *hai1a* morphant periderm-LifeActGFP embryos showed F-actin rings forming and contracting around periderm cells that were extruded apically from the epithelium. The cells surrounding an extruding cell formed rosettes (Fig. 3 A and Videos 2 and 3). Similar events occurred in the skin overlying the trunk (Fig. S2). Each extrusion event represented a single cell leaving the epithelium, but several cells in the same vicinity often underwent extrusion (Videos 2, 3, and 5). The formation of an actin ring around a cell that is "squeezed" to exit apically from an epithelial monolayer, leaving behind a rosette of surrounding cells, is characteristic of apical cell extrusion, a process normally used to eject apoptotic, damaged, or crowded cells while maintaining epithelial barrier function (Gudipaty and Rosenblatt, 2017).

To further explore this extrusion phenotype, we used the periderm-nuclear-EGFP line to determine the frequency of extrusion events and visualize nuclear morphology in extruded cells as an index of apoptosis (Videos 4, 5, and 6; and Fig. 3 B). In control embryos, <0.1% of cells in the field imaged extruded during the 28- to 46-hpf imaging period (Video 4 and Fig. 3, C and D). The rare cells that did extrude had grossly fragmented nuclei (Video 7 and Fig. 3 B), suggesting that extrusion from normal periderm reflects jettisoning of the occasional apoptotic cell. In periderm of *hai1a* morphants and mutants, the rate of extrusion increased to 4.3% and 4.4%, respectively, but only 0.1% and 0.4% of cells extruded with obvious nuclear fragmentation (Videos 5 and 8 and Fig. 3, C and D). However, the extruding cells in *hai1a* morphants and mutants often showed disappearance of nuclear EGFP fluorescence coincident with a uniform increase in fluorescence in the cytosol (Videos 5 and 8), suggesting possible disruption of the nuclear envelope late in the extrusion process (see Discussion).

Strikingly, in *par2b*−/− *hai1a* morphant embryos, only 0.3% of cells extruded during imaging (Video 6 and Fig. 3, C and D). Similarly, in *st14a*:*hai1a* double morphants, only 0.1% of cells extruded during the imaging period (Fig. 3, C and D). Overall, these results reveal matriptase- and Par2b-dependent apical cell extrusion of periderm cells in Hai1a-deficient embryos, suggesting that activation of Par2b by matriptase can directly or indirectly drive this important epithelial behavior.

Loss of cell–cell contacts, hypermobility, and swarming exhibited by basal layer keratinocytes in *hai1a* morphants is par2b dependent

Hai1a deficiency promotes basal cell migration (Carney et al., 2007). Accordingly, we examined the dependence of dynamics of such basal layer dynamics on *par2b* using the basal-layer-LifeActGFP line. Sequential images and 2-h time-lapse videos were acquired on live embryos 24–30 hpf. In control embryos, basal layer keratinocytes were stably apposed; 94% of cells maintained contact with one or more adjacent cells for >60 min (Fig. 4, A and E; and Video 9). In contrast, in *hai1a* morphant embryos, basal layer keratinocytes were usually not tightly apposed and extended filopodia and lamellipodia into the gaps between cells; only 9% of cells maintained stable cell–cell contacts (Fig. 4, B and E; and Video 10). Along with decreased cell–cell contact, cell movement was increased in *hai1a* morphants (Videos 10 and 11) compared with controls (Video 9), and centripetal movement or "swarming" of basal keratinocytes toward aggregations of the same was sometimes noted (Video 12). In *hai1a*:*st14a* double morphants, the basal
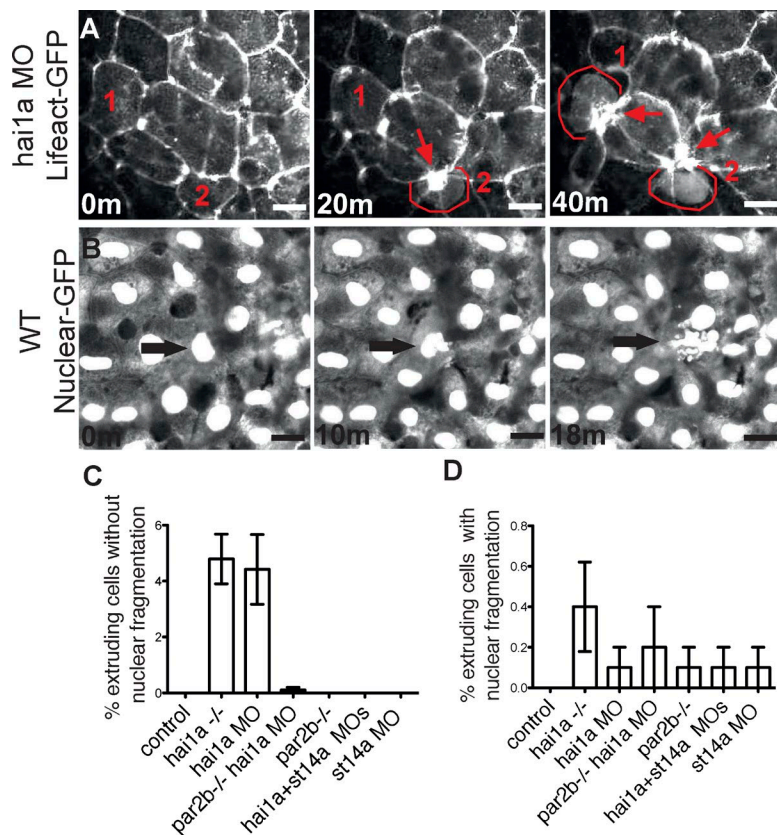
Figure 3. **par2b-dependent apical extrusion of epithelial cells from periderm in hai1a morphant embryos.** (A) The yolk sac periderm of a *hai1a* morphant periderm-LifeActGFP embryo was imaged from 28 to 46 hpf. Three time-lapse panels spanning 40 min show an F-actin ring that contracts around cells being extruded apically from the periderm. Cells destined to extrude are labeled 1 and 2 in all panels and are highlighted with red outline after extrusion has begun. Contracted actin rings remaining at the site of extrusion and at the center of rosettes formed by surrounding cells are marked by red arrows. Bar, 5 µm. (B) The yolk sac periderm of a control periderm-nuclear-GFP embryo was imaged from 28 to 46 hpf. Three panels spanning 18 min show extrusion of a cell with an obviously fragmented nucleus (arrow). Bar, 5 µm. (C and D) Quantitation of extrusion events in control and *hai1a* morphants with or without Par2b or matriptase (*st14a*) deficiency. The ventral yolk sac of 10 periderm-nuclear-GFP embryos for each condition was imaged from 28 to 46 hpf, and extrusion events were counted and classified by whether the nucleus of the extruding cell was not (C) or was (D) obviously fragmented. Results are expressed as the number of extrusion events as a percentage of the number of cells, usually ~200, present in the field at the start of the imaging period (mean ± SEM; $n = 10$). The *hai1a* morphant and mutant groups in C were different from all other groups by one-way ANOVA and Bonferroni posttest, $P < 0.0001$. No groups in D were different from control.

layer resembled that of controls; basal keratinocytes were tightly apposed and 88% maintained stable cell–cell contacts (Fig. 4, D and E; and Video 13). In *par2b⁻/⁻ hai1a* morphants, cells were more tightly apposed than in *hai1a* morphants, and 73% maintained stable cell–cell contacts compared with 9% in *hai1a* morphants and 94% in controls (Fig. 4, C and E; and Video 14). However, moving areas of increased LifeActGFP fluorescence suggesting increased F-actin dynamics were sometimes noted (Video 14). In the absence of *hai1a* MO, basal keratinocyte behavior in *par2b⁻/⁻* zebrafish was indistinguishable from that in wild type (Fig. 4). Collectively, these data show that loss of stable cell–cell contacts and hypermobility in *hai1a* morphants is matriptase-dependent and, in large part, *par2b*-dependent, suggesting that activation of Par2b by matriptase directly or indirectly helps drive this epithelial-mesenchymal transition-like behavior of basal layer.

Basal-layer-LifeActGFP embryos provided an opportunity to determine whether basal cells extrude in *hai1a* morphant embryos as periderm cells do. In contrast to *hai1a* morphants carrying fluorescent periderm markers, no extrusion of fluorescent cells was detected in the time-lapse studies of *hai1a* morphant basal-layer-LifeActGFP embryos described in Fig. 4. This observation suggests that apical cell extrusion in *hai1a* morphants was limited to the periderm.

Abnormal distribution of nuclei in periderm and basal layer in *hai1a* morphants is par2b dependent

Imaging for the periderm-nuclear-EGFP marker and immunostaining for the basal marker p63 was itself revealing. In contrast to the regular spacing of nuclei seen in controls, patches with increased numbers of nuclei per unit area were observed in both

periderm and basal layers in *hai1a* morphants. These "crowded" patches in periderm (Fig. 5 A) were colocated with crowded patches in the basal layer (Fig. 5 B), suggesting communication between layers. The crowded patches seen in still images corresponded to the areas of apical extrusion and remodeling of the periderm. These areas presumably also corresponded to the patches of hypermobility and swarming of basal keratinocytes seen with the basal-layer-LifeActGFP line described in Fig. 5 and Video 12. Crowded patches were not seen in the periderm or basal layer of *par2b⁻/⁻ hai1a* morphants (Fig. 5 and Fig. S3 A). The colocation of "crowding" in both layers with extrusion in periderm and hypermobility in the basal layer is again consistent with some linkage of these phenomena, and their common Par2b dependence suggests that activation of Par2b directly or indirectly drives remodeling, albeit of distinct types, in both layers.

Abnormal subcellular localization of E-cadherin in *hai1a* morphants is par2b dependent

Cell extrusion from the periderm and loss of cell–cell contacts and hypermotility in the basal layer suggest that cell–cell junctions are altered in both layers in *hai1a* morphants and mutants. E-cadherin distribution in periderm in *hai1a* morphants has not been studied. E-cadherin mislocalization in basal layer keratinocytes in *hai1a* morphants has been reported (Carney et al., 2007), but its dependence on *par2b* is unknown. Accordingly, we examined the pattern of E-cadherin immunostaining and its dependence on *par2b* in zebrafish embryos carrying the periderm-nuclear-EGFP marker and immunostained for the basal marker p63.

Immunostaining of *hai1a* morphants for E-cadherin revealed increased granular cytoplasmic staining in the basal layer clusters (Fig. 5 C), consistent with redistribution of E-cadherin
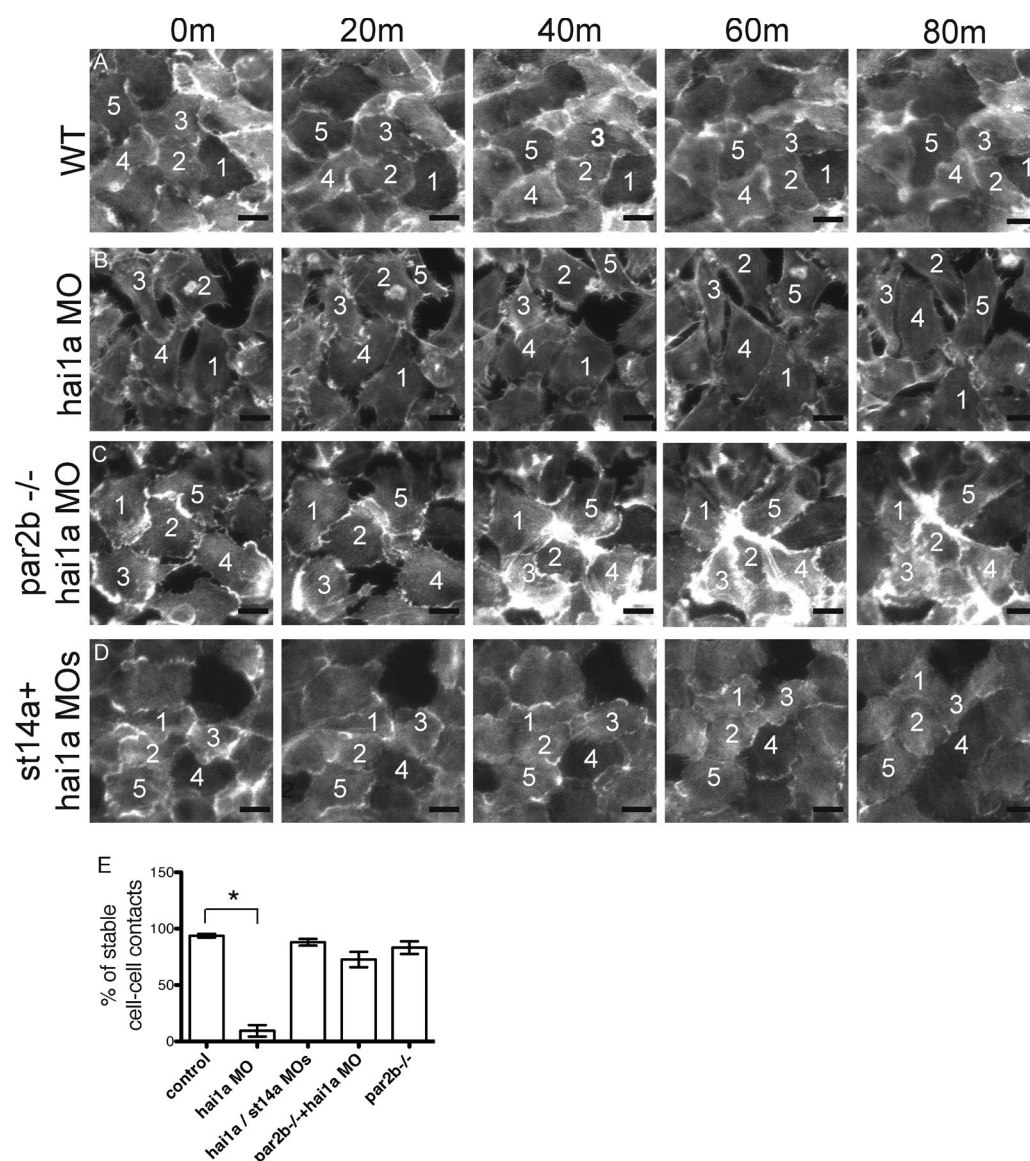
Figure 4. **Loss of cell–cell contacts and increased motility of basal layer keratinocytes in *hai1a* morphants is *par2b* dependent. (A–D)** The yolk sac basal layer of basal-layer-LifeActGFP control or *hai1a* morphant embryos with or without matriptase or Par2b deficiency was imaged between 24 and 30 hpf. Five panels spanning 80 min (m) are shown. **(A)** Control embryo. Note tightly apposed basal epithelial cells and stable relative positions of numbered cells. **(B)** *hai1a* morphant embryo. Note loss of cell–cell apposition and changing relative cell positions. **(C and D)** *par2b*⁻/⁻ *hai1a* morphant (C) and *st14a/hai1a* double morphant (D). Note increased cell apposition and decreased change in position compared with B. Bar, 1 µm. **(E)** Quantitation of stable cell–cell contacts in control and *hai1a* morphant basal-layer-LifeActGFP embryos with or without St14a or Par2b deficiency. Time-lapse images of a standard field over the ventral yolk sac were acquired from 24 to 30 hpf for 10 embryos for each condition, and the percentage of individual cells that maintained contact with a neighbor for at least 60 min was determined. Mean ± SEM (*n* = 10) is shown. Approximately 300 cell–cell contacts were analyzed per condition. The *hai1a* morphant group was different from controls (*, P < 0.0001), but other groups were not, by one-way ANOVA and Bonferroni posttest.

from junctions to intracellular vesicles and in agreement with published results (Carney et al., 2007). Importantly, mislocalization of E-cadherin and abnormal clustering of basal layer cells was absent in *par2b*⁻/⁻ *hai1a* morphants (Fig. 5). These data are in accord with the *par2b* dependence of loss of stable cell–cell contacts and increased cell motility in the basal layer of *hai1a* morphants (Fig. 4 and Videos 9, 10, 11, 12, 13, and 14).

E-cadherin mislocalization was also seen in *hai1a* morphant periderm in areas of clustering of periderm cell nuclei, and such mislocalization was largely absent in *par2b*⁻/⁻ *hai1a* morphants (Fig. S3 A). Thus, E-cadherin is indeed mislocalized in a manner consistent with disruption of adherens junctions in periderm and basal layer in *hai1a* morphants in a *par2b*-dependent manner.

Opposite effects of Par2b deficiency on BrdU incorporation in periderm versus basal layer in *hai1a* morphants

Increased cell proliferation in the basal layer in *hai1a* morphants has been reported (Carney et al., 2007). Additionally, although crowded patches were absent, we noted a relatively uniform increase in the overall number of nuclei in periderm of *par2b*⁻/⁻ *hai1a* morphants compared with *hai1a* morphants or controls (Fig. 5 A). Accordingly, we characterized cell proliferation as measured by BrdU incorporation in periderm and basal layer of *hai1a* morphants and its dependence on *par2b*.

Periderm-nuclear-EGFP embryos were incubated with BrdU from 28 to 31 hpf, washed, collected at 46 hpf, and immu-
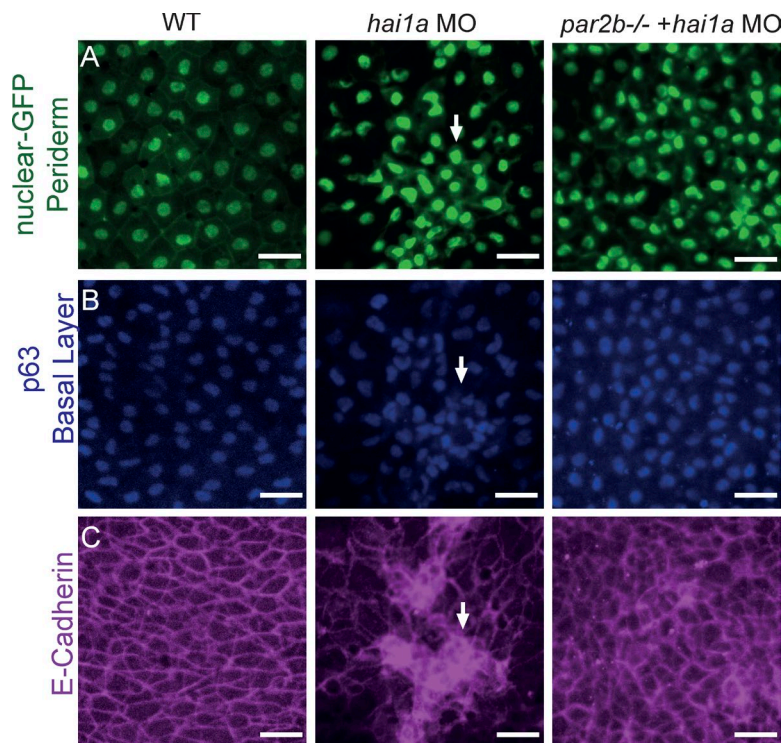
Figure 5. **Altered distribution of nuclei and E-cadherin in basal-layer keratinocytes in *hai1a* morphants and its *par2b*-dependence.** Control, *hai1a* morphant, and *par2b*⁻/⁻ *hai1a* morphant periderm-nuclear-GFP embryos were collected at 30 hpf, immunostained for the basal layer marker p63 and E-cadherin, and imaged by confocal fluorescence microscopy. **(A)** Nuclear-GFP marker of periderm cells. Note regular spacing in controls (left), clustered and crowded appearance in *hai1a* morphants (middle), and increased number in *par2b*⁻/⁻ *hai1a* morphants (right). **(B)** p63 marker for basal layer nuclei. Note regular spacing in controls (left), clustered and crowded appearance in *hai1a* morphants (middle), and more control-like pattern in *par2b*⁻/⁻ *hai1a* morphants (right). **(C)** E-cadherin staining in basal layer. Note localization to cell–cell junctions in controls (left), aberrant distribution with increased cytosolic staining in areas coinciding with clusters of p63-positive nuclei in *hai1a* morphants (middle), and more control-like pattern in *par2b*⁻/⁻ *hai1a* morphants (right). Bar, 20 µm.

nostained for BrdU and p63. Colocation of BrdU staining with nuclear EGFP was used to identify periderm layer cells that had incorporated BrdU; colocation with nuclear p63 staining was used to identify basal layer cells (Fig. 6, A and B).

In basal layer, 0.4% of nuclei were BrdU-positive in controls compared with 6.7% in *hai1a* morphant embryos (Fig. 6, A and D). In contrast, the percentage of basal layer nuclei labeled with BrdU in *hai1a* morphant embryos coinjected with *st14a* MO or deficient for Par2b was indistinguishable from control. Thus, increased BrdU incorporation in basal layer nuclei in *hai1a* morphants is *st14a* and *par2b* dependent, consistent with the notion that matriptase-driven Par2b activity contributes to proliferation of basal layer cells in this setting.

In periderm, 0.8% of nuclei were BrdU positive in controls compared with 4.0% in *hai1a* morphants and 0.3% in *hai1a* morphants coinjected with *st14a* MO (Fig. 6 C). Thus, as in the basal layer, loss of Hai1a function was associated with a matriptase-dependent increase in the fraction of periderm keratinocytes in S-phase. Surprisingly, in contrast to the basal layer in which increased BrdU labeling in *hai1a* morphants was prevented by Par2b deficiency, periderm in *par2b*⁻/⁻ *hai1a* morphant embryos showed a further increase in BrdU labeling, with 11% of nuclei BrdU positive compared with 4% in *hai1a* morphants without Par2b deficiency (Fig. 6 C). In accord with this result, there was an obvious increase in the fraction of periderm cells that underwent nuclear division in time-lapse imaging of *par2b*⁻/⁻ *hai1a* morphant embryos compared with *hai1a* morphant without Par2b deficiency or controls (Videos 4, 5, and 6).

Of note, BrdU labeling was also increased in periderm in *par2b*⁻/⁻ embryos compared with controls (5.0% vs. 0.8%), and injection of *par2b*⁻/⁻ *hai1a* morphant embryos with an *st14a* MO reduced the percent of periderm nuclei labeled from 11% in *par2b*⁻/⁻ *hai1a* morphant embryos to 1.7% (Fig. 6 C). At face value, these results suggest that matriptase promotes proliferation of periderm cells in *hai1a* morphants in a Par2b-independent

manner and that Par2b, rather than promoting proliferation as it does in the basal layer, inhibits proliferation in periderm.

Leukocyte infiltration of skin and increased inflammatory marker expression in hai1a morphants is par2b dependent

Leukocyte infiltration of skin and increased expression of *mmp9* and other inflammatory markers in *hai1a* morphant embryos has been reported (Carney et al., 2007; Mathias et al., 2007; LeBert et al., 2015). Infiltration of the fin fold with GFP-positive cells was readily seen in *hai1a* morphants in the *Tg (MPO:GFP)^uw* line, which expresses GFP in neutrophils, and such infiltration was absent in *par2b:hai1a* double morphants (Fig. S4). Similarly, expression of *mmp9*, *mmp13*, and *il1b* was increased in *hai1a* morphants, and such increases were *st14a* and *par2b* dependent (Fig. 7 A). These results suggest that matriptase-dependent Par2b activation directly or indirectly supports leukocyte infiltration and expression of markers and mediators of inflammation in the skin of *hai1a* morphants.

Matrix metalloproteinase (Mmp)–dependent components of the hai1a phenotype

Mmp activity can contribute to tissue remodeling (Page-McCaw et al., 2007), and Mmp9 depletion can partially rescue the appearance of skin clusters in *hai1a* morphants (LeBert et al., 2015). This result and our observation that increased Mmp expression in *hai1a* morphants is *par2b* dependent (Fig. 7 A) raised the possibility that Mmp activity might contribute to *par2b*-dependent features of the *hai1a* phenotype. Accordingly, we determined the effect of MO knockdown and pharmacological inhibition of Mmp9 and Mmp13 on apical cell extrusion in periderm, altered cell–cell contacts in the basal layer, and altered BrdU incorporation in periderm and in basal keratinocytes in *hai1a* morphants (Fig. 7, B–E). Although completely *par2b* dependent (Fig. 3), apical cell extrusion from periderm in *hai1a* morphants was not different in the absence or presence of *mmp9*
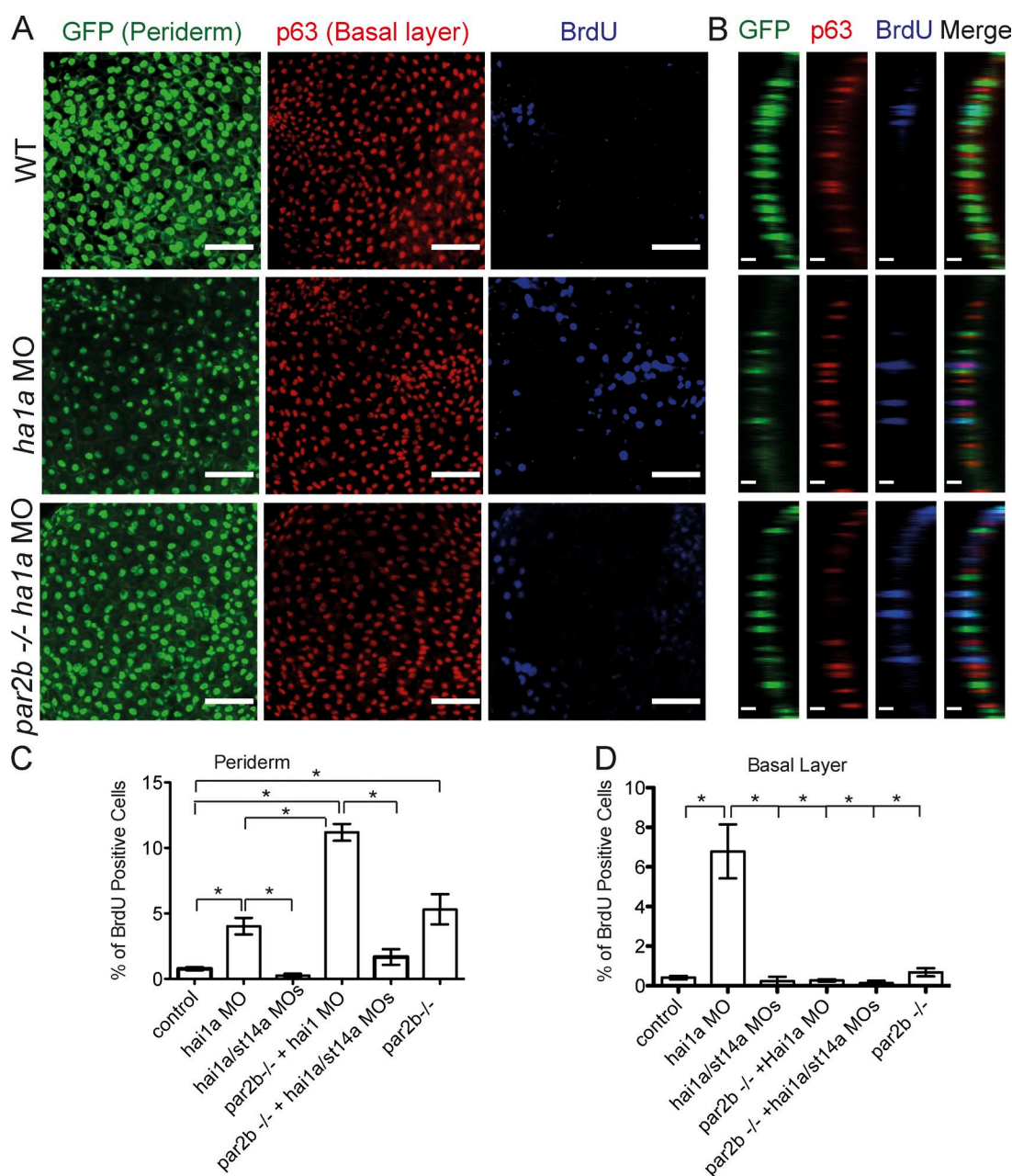
Figure 6. **Effect of Par2b deficiency on increased BrdU incorporation associated with loss of *hai1a* function in the basal layer versus periderm. (A and B)** Control and *hai1a* morphants periderm-nuclear-EGFP embryos with and without St14a or Par2b deficiency were incubated with BrdU for 3 h beginning at 28 hpf, collected for analysis at 46 hpf, and immunostained for p63 and BrdU. Bar, 50 µm. **(B)** Colocation of BrdU staining with either nuclear-GFP or nuclear p63 staining was used to identify periderm or basal layer cells that had incorporated BrdU, respectively. **(C and D)** The percentage of BrdU-positive nuclei in periderm (C) and basal layer (D) is shown (mean ± SEM of three experiments; for each experiment, 10 embryos were examined per condition, and 150–200 cells were analyzed in each embryo). Results were analyzed by one-way ANOVA and Bonferroni posttest. In C, the *hai1a/st14a* MO group and the *par2b*^{−/−} *hai1a/st14a* MO groups were not different from control; the *hai1a* MO group, the *par2b*^{−/−} group, and the *par2b*^{−/−} *hai1a* MO group were all different from control, and the *par2b*^{−/−} and *hai1a* MO groups were different from the *par2b*^{−/−} *hai1a* MO group (*, P < 0.05). In D, the *hai1a* MO group was different from all other groups (*, P < 0.0001).

MOs or Mmp9/13 inhibitor (Fig. 7 B). In contrast, exposure to Mmp inhibitors partially rescued stable cell–cell contacts in the basal layer in *hai1a* morphants (Fig. 7 C). Most strikingly, exposure to Mmp inhibitors mimicked the effects of Par2b deficiency on BrdU incorporation. Specifically, treatment of *hai1a* morphants with Mmp9/13 inhibitor prevented increased BrdU incorporation in the basal layer but augmented BrdU incorporation in periderm (Fig. 7, D and E). Mmp9 MOs had directionally

similar but smaller effects. At face value, these results suggest that Mmp9/13 activity contributes to altered cell–cell interactions and increased BrdU incorporation in the basal layer and to restraint of BrdU incorporation in periderm, and given *par2b*-dependent *mmp9* and *mmp13* expression in *hai1a* morphants, Par2b-induced Mmp expression may contribute to these phenotypes. Our experiments do not exclude the alternative that Mmp activity is simply permissive for these phenotypes.
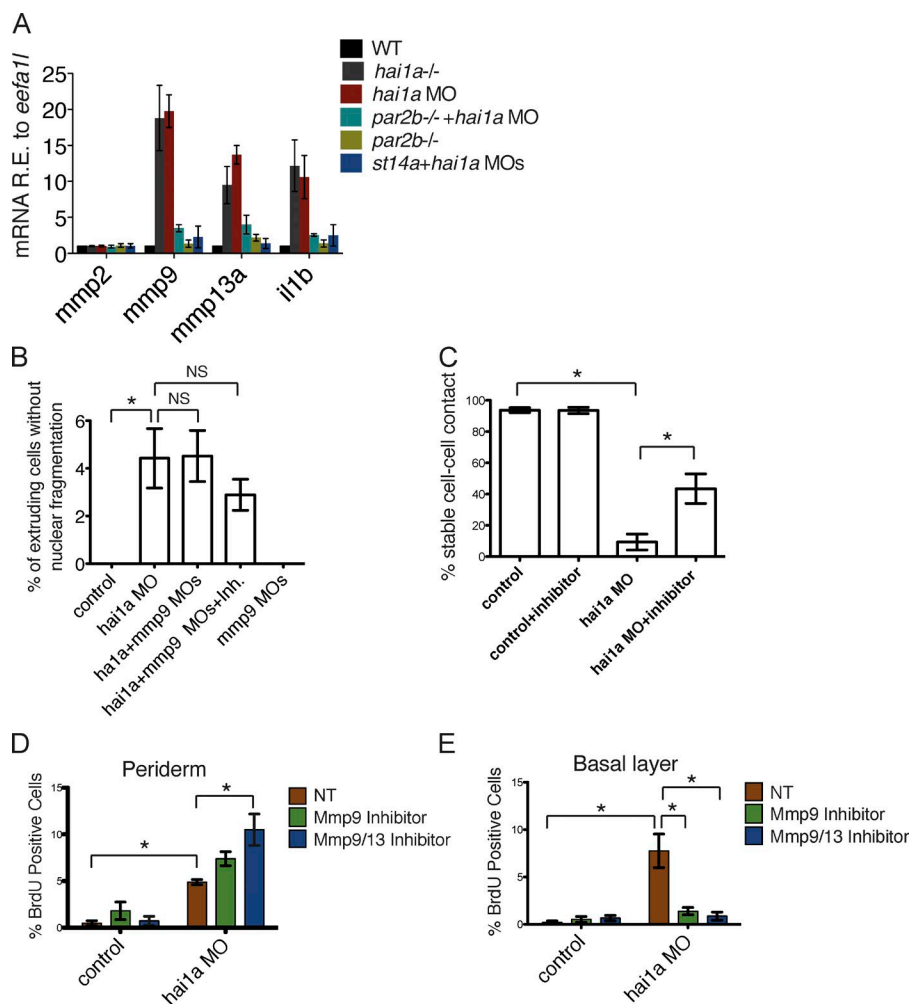
A

mRNA R.E. to *eefa1l*

Legend:
- WT (black)
- *hai1a-/-* (gray)
- *hai1a* MO (dark red)
- *par2b-/- +hai1a* MO (teal)
- *par2b-/-* (olive)
- *st14a+hai1a* MOs (dark blue)

x-axis: mmp2, mmp9, mmp13a, il1b

B

% of extruding cells without nuclear fragmentation

x-axis: control, hai1a MO, ha1a+mmp9 MOs, hai1a+mmp9 MOs+Inh., mmp9 MOs

C

% stable cell-cell contact

x-axis: control, control+inhibitor, hai1a MO, hai1a MO+inhibitor

D Periderm

% BrdU Positive Cells

Legend: NT, Mmp9 Inhibitor, Mmp9/13 Inhibitor

x-axis: control, hai1a MO

E Basal layer

% BrdU Positive Cells

Legend: NT, Mmp9 Inhibitor, Mmp9/13 Inhibitor

x-axis: control, hai1a MO

Figure 7. **Roles of *st14a* and *par2b* in *mmp9*, *mmp13*, and *il1b* expression and effects of Mmp inhibition in *hai1a* MO embryos. (A)** Controls, *hai1a* morphants, and mutant embryos with and without St14a or Par2b deficiency were collected at 30 hpf, and RNA was analyzed by quantitative RT-PCR. Expression relative to controls is shown (mean ± SEM, $n = 3$). **(B)** Control and *hai1a* morphant periderm-nuclear-EGFP embryos with or without mmp9 deficiency or mmp9/13 inhibition were imaged as in Fig. 3 (B–D). The percentage of cells without obvious nuclear fragmentation extruding in the field imaged (mean ± SEM; $n = 10$) is shown. Mmp knockdown and inhibition were without effect on increased extrusion in *hai1a* morphants by one-way ANOVA and Bonferroni posttest. NS, not significant. **(C–E)** Control and *hai1a* morphant basal-layer-Life-ActGFP embryos with or without Mmp9/13 inhibition were imaged and analyzed as in Fig. 4; mean ± SEM ($n = 10$ embryos/condition) is shown. Approximately 300 cell–cell contacts were analyzed per condition. Two-way ANOVA and Tukey posttest were used to analyze C–E. In C, the *hai1a* MO group was different from all other groups (*, P < 0.001). **(D and E)** Control and *hai1a* morphants periderm-nuclear-EGFP embryos with and without Mmp9 or Mmp9/13 inhibition were incubated with BrdU and analyzed as in Fig. 5. The percentage of BrdU-positive periderm cells (D) and basal layer cells (E) is shown (mean ± SEM; $n = 3$). In D, the *hai1a* MO groups were different from the control groups (*, P < 0.0001), and the Mmp9/13 inhibitor *hai1a* MO group was different from all other groups (*, P < 0.0001). In E, the *hai1a* MO without Mmp inhibitor treatment group was different from all other groups (*, P < 0.0001), and no other groups differed from control.

Effects of Erbb2 knockdown or EGF receptor (EGFR) inhibition on the *hai1a* phenotype

Like Hai1a-deficient embryos (Carney et al., 2007; this study), basal layer cells in *lgl2* mutant zebrafish embryos show E-cadherin redistribution and increased mobility (Reischauer et al., 2009). These *lgl2* phenotypes are prevented by Erbb2 deficiency (Reischauer et al., 2009). G protein–coupled receptors including Par2 can promote EGFR activation by an incompletely understood mechanism dubbed transactivation (Chung et al., 2013; Wang, 2016). Thus, it is plausible that transactivation of Erbb2 by Par2b might contribute to the *hai1a* phenotype. To explore this hypothesis, we investigated the effect of *erbb2* MO and the EGFR inhibitor PD168393 on the *hai1a* phenotype. PD168393 treatment did not reduce apical extrusion of cells lacking nuclear fragmentation from the periderm in *hai1a* morphant embryos (Fig. 8 A), nor did it reverse E-cadherin redistribution to endosomes in periderm (Fig. S3 B). Unexpectedly, however, PD168393 treatment of *hai1a* morphant embryos was associated with a marked increase in apical extrusion of periderm cells with obvious nuclear fragmentation (Fig. 8 B). PD168393 treatment did not increase cell extrusion in control embryos. The dose of *erbb2* MO was limited by side effects; at the dose used, its effects mimicked those of PD168393 treatment directionally but did not reach statistical significance. These results suggest that Erbb2 activation does not contribute to live apical cell extrusion in Hai1a-deficient embryos but that Erbb2 or another PD168393 target may be necessary for survival of cells in Hai1a-deficient periderm. Of note, Par2b deficiency blunted the increase in extrusion of cells with fragmented nuclei in Hai1a-deficient PD168393-treated embryos, suggesting that Par2b signaling may contribute to increased apoptosis and/or for extrusion in this setting.

erbb2 MO or PD168393 treatment had no effect on increased BrdU labeling of periderm cells in *hai1a* morphants, but both markedly attenuated the increased BrdU labeling seen in the periderm of *par2b−/− hai1a* morphants (Fig. 8, D and E). Indeed, combined Par2b deficiency and Erbb2 inhibition produced a virtually complete reversal of the *hai1a* periderm phenotype. Collectively, our results are consistent with the notion that Erbb2 activity supports survival of periderm cells in *hai1a* morphants with intact *par2b* function and proliferation of periderm cells in *hai1a* morphants lacking *par2b* and extrusion. Additionally, the observation that *erbb2* MO and PD168393 blocked proliferation in Hai1a-deficient periderm lacking *par2b* suggests that Erbb2 plays a Par2b-independent role in regulating proliferation of these cells (Fig. 9 A).

In the basal layer, *erbb2* MO and PD168393 treatment blunted the increased BrdU labeling in *hai1a* morphants (Fig. 8, F and G). PD168393 treatment also prevented loss of stable cell–cell contacts and hypermotility in the basal layer in *hai1a* morphants (Fig. 8 C). Thus, like Par2b, Erbb2 appears to be required for increased cell proliferation and altered cell–cell adhesion in the basal layer of *hai1a* morphants and may mediate or be permissive for these behaviors (Fig. 9 B).
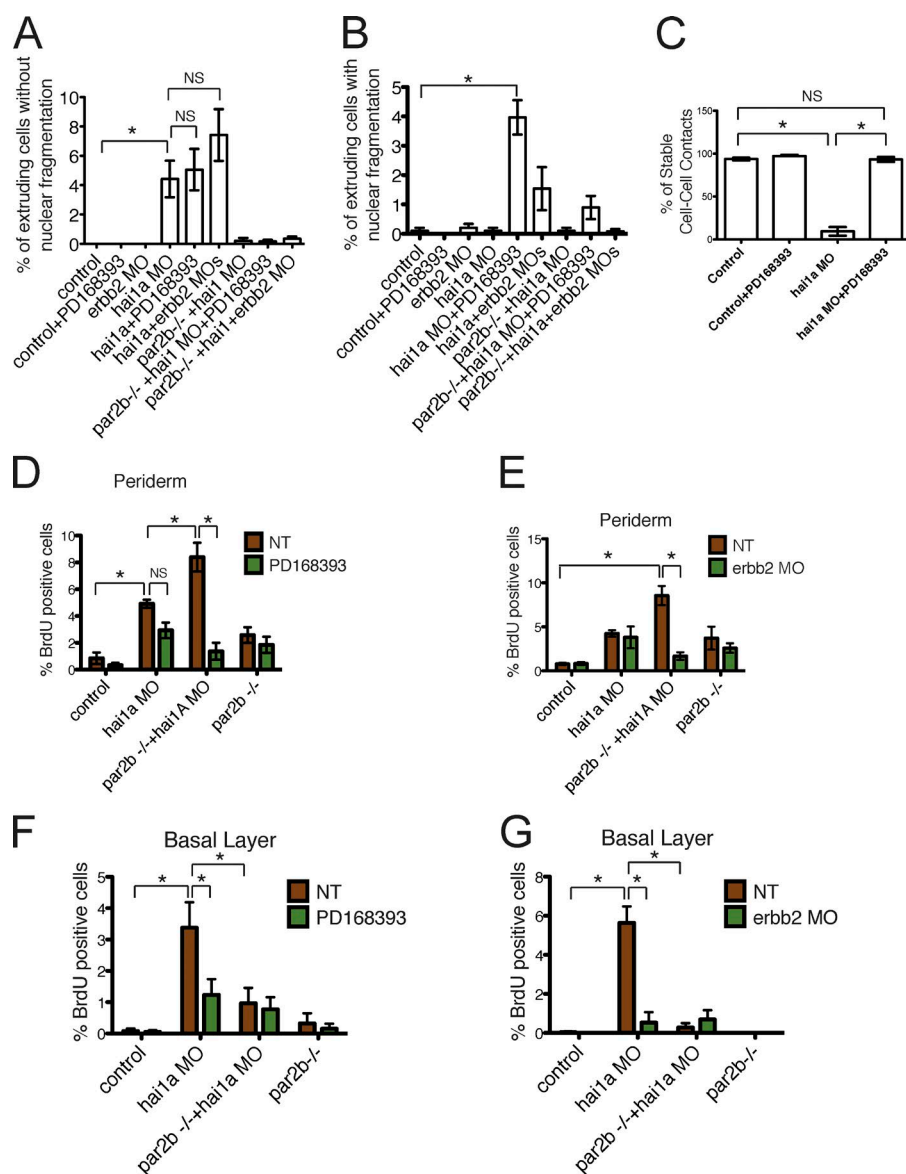
Figure 8. **Effect of Erbb2 and EGFR inhibition on the *hai1a* phenotype. (A and B)** Control and *hai1a* morphant periderm-nuclear-EGFP embryos with or without injection of *erbb2* MO, treatment with the EGFR inhibitor PD168393 or *par2b* deficiency were imaged and analyzed as in Fig. 3. Percentage of cells undergoing extrusion without (A) and with (B) obvious nuclear fragmentation (mean ± SEM; $n = 10$) is shown. In A, the hai1a MO, hai1a MO plus PD168393, and hai1a erbb2 MO groups were different from control but not from each other by one-way ANOVA and Bonferroni posttest (*, $P \leq 0.05$). No other groups were different from control. In B, the hai1a MO PD168393 group was different from control (*, $P < 0.0001$). **(C–G)** Control or *hai1a* morphant basal-layer LifeActGFP embryos without or with PD168393 treatment were imaged and analyzed as in Fig. 4. Percentage of cells in the field imaged that maintained stable cell–cell contact (mean ± SEM; $n = 10$) is shown. Two-way ANOVA and Tukey posttest were used to analyze C–G. In C, the *hai1a* MO group was different from control and from the other groups (*, $P < 0.0001$). Control and *hai1a* morphant periderm-nuclear-EGFP embryos without or with PD168393 treatment (D and F) or erbb2 MO treatment (E and G) were labeled with BrdU and analyzed as in Fig. 6. The percentage of cells labeled with BrdU (mean ± SEM; $n = 3$) in periderm (D and E) and basal layer (F and G) is shown. In D, the *hai1a* MO and *hai1a* MO *par2b*$^{-/-}$ groups were different from control and from each other (*, $P < 0.05$). PD168393 treatment had a significant effect overall, and the *hai1a* MO *par2b*$^{-/-}$ ± PD168393 groups were different (*, $P < 0.0001$). The same result was obtained in E with *erbb2* MO. In F and G, the *hai1a* group was different from all other groups (*, $P < 0.05$ in F; *, $P < 0.0001$ in G). NS, not significant.

Discussion

Matriptase provides local trypsin-like serine protease activity on the surface of epithelial cells (List et al., 2009; Buzza et al., 2010). Matriptase is negatively regulated by Hai1 and Hai2 (Oberst et al., 2005; Szabo et al., 2009; Nonboe et al., 2017). We and others have provided evidence that matriptase and its regulators can modify epithelial cell behavior in part via Par2 (Bocheva et al., 2009; Camerer et al., 2010; Sales et al., 2015b; Le Gall et al., 2016). Gain-of-function for matriptase, its activators, or Par2 can trigger chronic inflammatory and proliferative responses in mouse skin, in some models leading to squamous cell carcinoma (Steinhoff et al., 2003; Bocheva et al., 2009; Frateschi et al., 2011; Cheng et al., 2014). However, the roles of Par2 in regulating epithelial cell behavior and their relationships to matriptase activity have been incompletely explored.

Hai1a-deficient skin in zebrafish embryos has been put forward as a model of chronic inflammation (Mathias et al., 2007). It can also be viewed as a model of epithelial remodeling. Using this model, we identified and characterized Par2-dependent responses. Our studies unexpectedly revealed classic epithelial apical cell extrusion as a feature of this model and demonstrated that this behavior is Par2 dependent. Roles for Par2 in regulating cell proliferation that were opposite in distinct but adjacent epithelial monolayers, and roles in regulating cell–cell junctions, mobility, survival, and expression of genes involved in tissue remodeling and inflammation, were also uncovered. These are epithelial cell behaviors that contribute broadly to embryonic development, homeostasis, inflammation and reparative responses, and because Hai1, matriptase, and Par2 are co-expressed in most mammalian epithelia (Camerer et al., 2010), the actions of matriptase-driven Par2 activity in zebrafish skin likely have counterparts in other tissues and settings.

Our observations are summarized in Table S2. As previously reported, the basal layer of Hai1a-deficient embryos showed a redistribution of E-cadherin, loss of cell–cell contacts, and increased cell motility as well as increased BrdU labeling, all of which were matriptase dependent (Carney et al., 2007). We show that all of these phenotypes are also Par2b dependent. Further, our data suggest that Hai1a, matriptase, and Par2b are coexpressed in basal layer cells and that zebrafish matriptase can cleave zebrafish Par2b at its activating cleavage site like
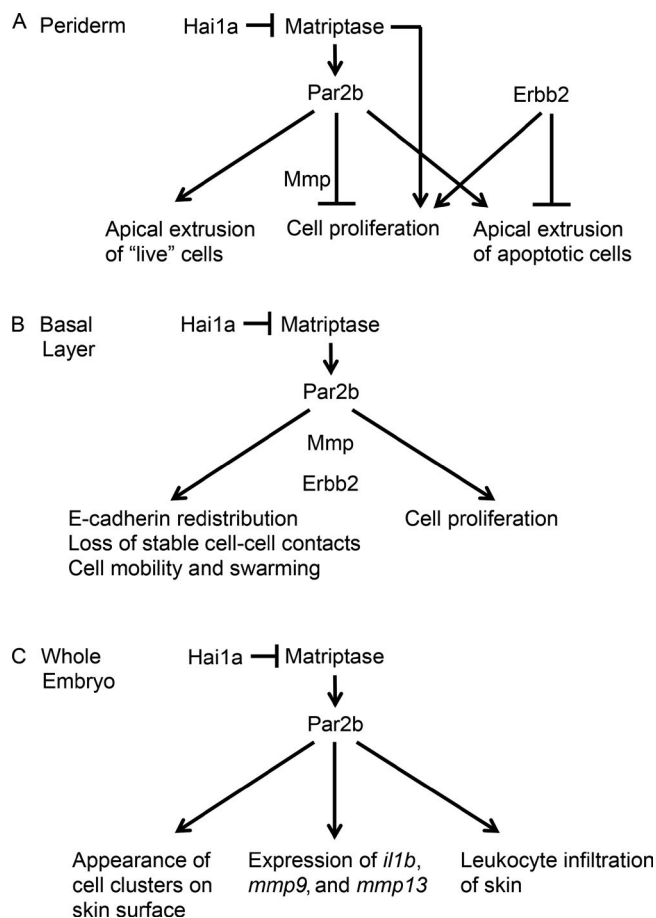
Figure 9 (left column)

A Periderm

Hai1a ⊣ Matriptase

Matriptase → Par2b

Par2b → Apical extrusion of "live" cells

Mmp

Par2b / Matriptase / Erbb2 → Cell proliferation

Erbb2 ⊣ Apical extrusion of apoptotic cells

B Basal Layer

Hai1a ⊣ Matriptase

Matriptase → Par2b

Mmp
Erbb2

Par2b → E-cadherin redistribution / Loss of stable cell-cell contacts / Cell mobility and swarming

Par2b → Cell proliferation

C Whole Embryo

Hai1a ⊣ Matriptase

Matriptase → Par2b

Par2b → Appearance of cell clusters on skin surface

Par2b → Expression of *il1b*, *mmp9*, and *mmp13*

Par2b → Leukocyte infiltration of skin

Figure 9. **Summary of effects and working models.** Hai1 can inhibit matriptase, matriptase can activate Par2, and loss of Hai1 function in zebrafish is associated with matriptase-dependent skin phenotypes. We characterized the role of Par2b in the two distinct epithelial layers that comprise skin, periderm, and basal layer in Hai1a-deficient embryos. **(A)** Par2b is necessary for apical extrusion of apparently live cells from the periderm of Hai1a-deficient embryos and for apical extrusion of apoptotic cells in such embryos in which the EGFR Erbb2 is inhibited. Par2b also negatively regulates periderm cell proliferation. Mmp activity is necessary for the latter but not for apical extrusion. Erbb2 is necessary to prevent periderm cell apoptosis and associated additional extrusion events in Hai1a-deficient embryos and for high levels of cell proliferation in such embryos lacking Par2b. Combined deficiency or inhibition of Par2b and Erbb2 caused a nearly complete rescue of the Hai1a phenotype. At face value, these and other results suggest that matriptase-driven Par2b activity can drive apical cell extrusion and suppress proliferation in the periderm; that matriptase and Erbb2 promote periderm cell proliferation by a Par2b-independent mechanism; and that Erbb2 promotes survival of periderm cells in the setting of Hai1a-deficiency. **(B)** Par2b is necessary for and may drive E-cadherin redistribution, loss of stable cell–cell contacts, and increased cell movement and proliferation in the basal layer. These basal layer behaviors were partially dependent on Mmps and Erbb2. Thus, these molecules may mediate the effects of Par2b activation or play a permissive role. **(C)** Par2b is necessary for several phenotypes measured at the whole-embryo level: appearance of cell clusters on skin, leukocyte infiltration of the skin, and induction of *il1b*, *mmp9*, and *mmp13* expression. The latter might contribute to phenotypes in A or B. The cell clusters almost certainly reflect basal cell swarming and areas of increased cell density and extrusion in periderm, which tended to be colocated. Collectively, these results are consistent with a model in which a local Hai1-matriptase-Par2 system may mediate responses to altered epithelial integrity.

the cognate mammalian proteins (Camerer et al., 2010). Transplantation experiments by Carney et al. (2007) suggest that loss of normal cell–cell contacts and increased movement of

basal layer cells associated with Hai1a deficiency is basal cell autonomous. Par2 is an efficient activator of Rac, and hence of F-actin organization in lamellipodia, which drives cell migration (Camerer et al., 2010; Shi et al., 2013). Par2 activation is also associated with loss of E-cadherin adhesion in airway epithelial cells (Winter et al., 2006), and Par2 can promote cell proliferation in some settings (Hirota et al., 2005; Hu et al., 2013; Sales et al., 2015b). Thus, a parsimonious model is that loss of Hai1a function in basal layer cells leads to increased activity of matriptase and Par2b activation in these same cells, with Par2b then promoting E-cadherin redistribution, loss of cell–cell contact, motility, and proliferation (Fig. 9). This model does not exclude participation of other Hai1a targets or matriptase substrates. For example, matriptase can cleave EpCam in vitro, and mutation of *epcam* in zebrafish triggers cell shedding and proliferative defects (Slanchev et al., 2009; Wu et al., 2017).

Increased *il1b*, *mmp9*, and *mmp13* expression and leukocyte infiltration of the fin fold in Hai1a-deficient zebrafish embryos were also *par2b* dependent. Thus, like the basal layer responses, this inflammatory response fits a simple matriptase-driven Par2b activity–dependent model (Fig. 9). Depletion of leukocytes does not prevent the gross skin phenotype associated with Hai1a deficiency (Carney et al., 2007; Mathias et al., 2007) suggesting that, although leukocyte infiltration is downstream of Par2b, it does not cause the other Par2-dependent structural and functional abnormalities seen in the skin of Hai1a-deficient zebrafish embryos. *par2b*-dependent induction of interleukin-1b (Fig. 7 A) and other cytokines and chemokines or *par2b*-dependent disruption of barrier function may trigger leukocyte infiltration. Our results in zebrafish are consistent with previous observations suggesting that matriptase and Par2 activity can promote inflammatory responses in mouse skin (Frateschi et al., 2011) and suggest that leukocyte infiltration may not be causal for proliferative and other skin phenotypes in these models.

The periderm of Hai1a-deficient embryos has not been previously studied in detail and revealed several distinct and surprising behaviors. One was apical cell extrusion that was matriptase- and Par2b-dependent. Classically, apical cell extrusion from an epithelium is triggered by apoptosis, damage, or cell crowding (Eisenhoffer et al., 2012; Gudipaty and Rosenblatt, 2017). The nuclei of periderm cells extruding in Hai1a-deficient embryos were not grossly fragmented. Extruding cells did show evidence of nuclear envelope breakdown, but this occurred late in the extrusion process. Thus, apical cell extrusion in this model is probably not initiated by apoptosis, but extruding cells may undergo anoikis.

Interestingly, treatment with Erbb2 inhibitors doubled the already high rate of apical extrusion of periderm cells in Hai1a-deficient embryos, and this increase was attributable to extrusion of cells with already grossly fragmented nuclei. Such extrusion was also Parb2 dependent. Thus, our results suggest that Par2b activity contributes to apical extrusion of both live and apoptotic cells (Fig. 9). Par2b is an efficient activator of Rac and F-actin assembly (Shi et al., 2013), and our data are consistent with a simple model in which matriptase-driven Par2b activity in periderm helps drive cell extrusion directly. Par2 is a G protein–coupled receptor (GPCR), and S1pr2, a GPCR for sphingosine-1-phosphate, can also stimulate apical extrusion in MDCK monolayers and zebrafish epidermis (Gu et al., 2011). Thus, different GPCRs may contribute to extrusion in different settings.

Our studies do not exclude participation of other matriptase substrates or less direct mechanisms of Par2b-driven extrusion. For example, cell crowding can drive apical cell extrusion (Eisenhoffer et al., 2012; Gudipaty and Rosenblatt, 2017), sites with an increased rate of extrusion in periderm were colocated with crowded patches of periderm cells, and the formation of such patches was Par2b dependent. Thus, it is possible that Par2b activity first drives periderm remodeling and cell crowding, with the latter helping to drive extrusion. However, embryos deficient in Hai1a and Par2b showed markedly less extrusion than Hai1a-deficient embryos despite increased periderm cell proliferation and a relatively uniform increase in cell density. Thus, crowding, at least as occurs in Hai1a-Par2b-deficient periderm, is not sufficient to drive extrusion.

Areas of apical cell extrusion and increased cell density in periderm were also colocated with areas of increased cell density in the basal layer, suggesting crosstalk between layers. Mmp or Erbb2 inhibition substantially reversed the basal layer phenotypes of decreased cell–cell contact and increased mobility and proliferation in Hai1a-deficient embryos without blocking apical cell extrusion or increased proliferation in periderm (Table S2). Thus, periderm phenotypes can occur in the absence of basal layer phenotypes. Similarly, previous transplantation studies suggest that basal layer phenotypes in Hai1a-deficient embryos are cell autonomous (Carney et al., 2007) and may occur in the absence of periderm phenotypes. Overall, it appears that matriptase- and Par2b-driven epithelial cell behaviors in each layer may be partly autonomous but coordinated by cross-talk. Potential mechanisms for cross-talk that promotes colocation are discussed later in this article.

In contrast to its effects in the basal layer, Par2b deficiency alone was associated with increased BrdU incorporation in periderm. Further, BrdU incorporation in periderm of embryos lacking both Hai1a and Par2b was increased compared with embryos lacking either Hai1a or Par2b alone. Interestingly, matriptase knockdown largely prevented increased BrdU incorporation in this setting. Thus, as in the basal layer, matriptase activity promotes proliferation of periderm cells but, unlike in the basal layer, Par2b appears to inhibit rather than mediate cell proliferation. These results suggest that matriptase promotes periderm cell proliferation via a substrates other than Par2b. Additionally, opposite roles for Par2b in regulating proliferation in adjacent epithelial structures raises the possibility that this system contributes to a remodeling or differentiation process that must coordinate proliferation across cell types.

Although the periderm and basal layers in zebrafish embryo skin represent distinct lineages (Le Guellec et al., 2004) and apical layers are derived from the basal layer in mouse (Simpson et al., 2011), zebrafish embryo and mouse skin both have apical layers comprised of differentiated squamous cells and basal layers that are more stem-like. Interestingly, Par2 overexpression in basal stem cells in mouse skin is associated with tumorigenesis, but Par2 overexpression in squamous cells inhibits proliferation (Rattenholl et al., 2007; Sales et al., 2015b). Thus, our findings suggest that a functionally analogous system featuring inhibition of apical squamous cell proliferation and stimulation of basal cell proliferation by Par2b is conserved across these species and settings.

Mmps contribute to the Hai1a skin phenotype (LeBert et al., 2015). We observed that induction of Mmp9 and Mmp13 expression in Hai1a-deficient embryos is Par2b dependent, and that Mmp9 and Mmp13 inhibition mimicked the effects of

Par2b deficiency in the basal layer. Thus, Par2b-driven increases in Mmp9 and Mmp13 expression by basal cells may contribute to loss of cell–cell contacts and increased motility and proliferation of basal layer cells in Hai1a-deficient embryos. Our studies do not exclude a less direct mechanism or a permissive role for Mmp9 and Mmp13 activity in these phenotypes.

In periderm, Mmp9 and Mmp13 inhibition mimicked the effect of Par2b deficiency on BrdU incorporation. Given that increased Mmp expression was Par2b dependent, this observation raises the possibility that Par2b-driven increases in Mmp activity may contribute to inhibition of proliferation in periderm. In contrast, and perhaps surprisingly, Mmp9 and Mmp13 inhibition had no effect on apical cell shedding in Hai1a-deficient embryos, suggesting that activity of these proteases is unnecessary for this process.

The matriptase- and Par2-driven Erbb2-dependent phenotypes we observed in zebrafish skin may have parallels in human cancer cells. Par2 activation is associated with Mmp- and EGFR-dependent ERK activation and proliferation in a colon cancer cell line, and "transactivation" of EGFR by Par2 has been suggested to contribute to these phenotypes (Darmoul et al., 2001, 2004). Par2 has also been reported to promote survival of an adenocarcinoma-derived lung epithelial cell line by transactivation of EGFR (Michel et al., 2014). These results raise the possibility that Par2b-dependent activation of Erbb2 might contribute to Erbb2-dependent cell proliferation in basal layer and cell survival in periderm in Hai1a-deficient zebrafish skin. However, the ability of *erbb2* MO and PD168393 to reverse the increased BrdU incorporation in Hai1a-deficient periderm lacking Par2b suggests that Erbb2 is acting in a Par2b-independent manner in this setting, and that Hai1a- and matriptase-dependent, Par2b-independent mechanisms of Erbb2 activation in this system remain to be uncovered.

The mechanism by which matriptase activity is regulated in normal physiology is not fully understood. In at least some polarized epithelial cell types, the matriptase activator prostasin traffics to the apical cell membrane, whereas matriptase is basolateral (Buzza et al., 2013). Because these proteases can mutually activate, loss of junctional integrity and polarity resulting in altered protease localization might trigger their activation. Given that matriptase gain of function leads to E-cadherin redistribution and loss of cell–cell junctions (Buzza et al., 2010) and our finding that these activities are Par2b dependent in zebrafish embryo skin, a positive feedback loop might exist in which matriptase and Par2b activity begets loss of junctions and polarity with altered trafficking that begets more local matriptase and Par2b activity. Further, Hai1a is partially redundant with Hai1b in zebrafish skin (Carney et al., 2007). Thus, the matriptase system in Hai1a morphant embryos is only partially activated at baseline, but it may be more sensitive to activation and amplification mechanisms. Such a sensitized self-amplifying system might allow mechanical or biochemical signals, perhaps inducing cytokines or Mmps or shed matriptase itself to act between layers and drive the colocation of patches of affected epithelium in basal and periderm layers observed in our studies.

The Par2b-dependent responses that were triggered by Hai1a deficiency in our studies—apical cell shedding in the periderm; loss of cell–cell contacts, mobility, and proliferation in the basal layer; and cytokine and Mmp production—would make sense as an initial response to injury, and the notion that activation of matriptase and Par2b in this system might normally be initiated by local injury sensed as loss of epithelial

integrity or polarity would fit such a model. The zebrafish skin offers a tractable system to test these ideas by future studies to determine where and when matriptase and Par2b are activated, their cell-autonomous roles in distinct epithelial behaviors, and their importance in responses to epithelial perturbations. Use of this system to further understand the roles of Par2 may illuminate mechanisms contributing to epithelial homeostasis and disease and help guide preclinical and clinical studies of drugs targeting this receptor (Yau et al., 2013).

Materials and methods

Nomenclature

Matriptase is also known as MTSP1 and St14. The zebrafish matriptase homologue St14a (gene symbol *st14a*) was studied here. In general, we refer to the protein encoded by *st14a* as matriptase and the gene as *st14a*. Hepatocyte-activator inhibitor 1 (Hai1) is also known as Spint1. The zebrafish Hai1 homologue Hai1a, also known as Spint1a (gene symbol *hai1a* or *spint1a*), was studied here. Par2 is also known as F2rl1. The zebrafish Par2 homologue Par2b, also known as F2rl1.2 (gene symbols *par2b* or *f2rl1.2*), was studied here.

par2b and st14a constructs

Zebrafish *par2b* and zebrafish *st14a* cDNAs were obtained from GE. The Par2b cleavage reporter AP-Par2b was generated in a manner analogous to previous mammalian versions (Ludeman et al., 2004; Camerer et al., 2010). In brief, zebrafish *Par2b* was amplified by PCR using primers 5′-GGCCGGATCCACCATGGCGGTGTCCGAGA-3′ and 5′-GGCCGCGGCCGCTCAGCAAGTGCTGGTTTCCGTGTT-3′ and inserted between the BamH1 and Not1 sites in pcDNA3.1, or using the primers 5′-GGCCGTTAACGCCCAGCCAGGCAAAAATGG-3′ and 5′-GGCCGTTAACGCAAGTGCTGGTTTCCGTGTT-3′ and inserted at the HapI site in pCMV-SEAP. A *Par2b* cleavage site mutant version of AP-Par2b was made using the primers 5′-GGCCGGATCCACCATGGCGGTGTCCGAGAGCTACAGGGATTTTATTATTTTTGGCGTGTGTCATTTTTGCTTCTGCCCAGCCAGGCAAAAATG-3′ and 5′-GGCCTCTAGATCAGCAAGTGCTGGTTTCC-3′. The PCR product was used to generate a BamHI and XbaI fragment to replace the cognate fragment in AP-Par2b.

Zebrafish *st14* was amplified by PCR using primers 5′-GGCCGGATCCACCATGGACCCTATGGATGGAGGAAT-3′ and 5′-GGCCGCGGCCGCTTACACTCCCGTCTTCTCCTT-3′ and subcloned between the BamHI and NotI sites in pcDNA3.1. Constructs were confirmed by sequencing. Enzymes were from New England Biolabs.

AP release assay

HEK 293T cells were plated in DMEM with 10% FBS at a density of 0.5 × 10^5 cells/well of a 24-well plate. Approximately 24 h later, cells were left untransfected or transfected with empty pcDNA3.1 or pcDNA3.1 constructs directing expression of AP-Par2b with a wild-type or mutated cleavage site and/or *st14a*. Approximately 24 h later, wells were washed once with 0.5 ml DMEM medium containing 0.1% BSA and 20 mM Hepes, and 300 µl medium was added to each well and incubated for 45 min at 37°C. 200 µl medium was removed and transferred to labeled tubes kept on ice. The remaining 100 µl was removed from the wells and cells washed once with 0.5 ml medium. 300 µl fresh medium containing 0.1 µg/ml trypsin (TPCK treated; Sigma-Aldrich) was added to each well and incubated for 10 min at 37°C. 200 µl of the trypsin-containing medium was removed from the wells and kept on ice. The samples from pre- and post-trypsin treatments were centrifuged at 13,000 rpm for 10 min, and 60 µl of each sample was added to 180 µl of 1× sample dilution buffer from the Tropix kit (Applied Biosystems) and heated for 30 min at 65°C. Samples were then cooled to room temperature, and 50 µl of each was added to 50 µl assay buffer in a 96-well plate in triplicate and incubated for 5 min at room temperature. 50 µl reaction buffer containing AP chemiluminescent substrate (Tropix kit) was added to each well and incubated further for 20 min. Chemiluminescence was measured in a microplate luminometer (Promega Glo Max). Where indicated, total expression of AP-Par2b constructs was assessed by lysing cells in 250 µl of 0.2% Triton X-100 24 h after transfection; 15 µl lysate was added to 185 µl Tropix buffer, which was then processed as just described to measure AP activity.

Zebrafish maintenance and strains

Zebrafish were maintained and handled in compliance with standard (http://zfin.org) and University of California, San Francisco Institutional Animal Care and Use Committee protocols. Wild-type strains used were TL, AB, and EKW. The *par2b* mutant line was outcrossed twice to each of these strains and to four of the transgenic lines; in all backgrounds, Par2b deficiency rescued the *hai1a* morphant skin phenotype as described in Results. Published transgenic lines were *Tg (krt4:nlsEGFP)cy34* (Chen et al., 2011), Tg (krt4:Sce.Abp140 -Venus)cy22 (Chen et al., 2011), Tg (UAS:Lifeact-GFP)mu271 (Helker et al., 2013), *TgBAC (ΔNp63:Gal4FF)la213* (Rasmussen et al., 2015), *Tg (MPO:GFP)uw* (Mathias et al., 2006), and *Hai1a* Mutant Line: *spint1lhi2217* (Carney et al., 2007; Mathias et al., 2007).

Injections and MOs

MOs were obtained from Gene Tools. 2 nl of MO solution was injected at the one- to two-cell stage. Sequences and concentrations were as follows: *Hai1a* MO: 5′-ACCCTGAGTAGAGCCAGAGTCATCC-3′, 50 mM (Carney et al., 2007); *Par2b* (*f2rl1.2*) MO: 5′-ATTCCGCTTTTTCCTCTAGTACTCC-3′, 100 mM; *matriptase1a* (*st14a*) MO: 5′-AACGCATTCCTCCATCCATAGGGTC-3′, 100 mM (Carney et al., 2007); *mmp9* MO1 5′-GAATAATGTCCCACCTGTATGTGAC-3′, 50 mM (Volkmann et al., 2010); *mmp9* MO2 5′-GTAAGTTTACCTCTGTTAGGGCAGA-3′, 50 mM (Volkmann et al., 2010); and *erbb2* MO: 5′-GTCCGCCTCCATCGATTATTCCTCC-3′, 50 mM (Lyons et al., 2005).

Generation of par2b (f2rl1.2) mutant

The design of the TALEN effectors was done with the web tool at https://tale-nt.cac.cornell.edu/. TALEN constructs were assembled using the Golden Gate TALEN and TAL Effector kit 2.0 according to Cermak et al. (2011) (Addgene). Two Target sequences were used for exon 2: 5′-TACACCCAGCTGCCATTTACATGGGCAACCTGGCACTTGCAGACCTG-3′ and 5′-TATGGCGAGGAGATGTGCAAAGTATCAGTGGGCTTCTTCTACGGGAACATGTA-3′ (spacer sequence underlined). TALEN effector mRNAs were synthesized using the Ambion mMessage mMachine T7 Ultra kit (Applied Biosystems) and injected at the one-cell stage. The experiments were done with F2 and subsequent generations.

Drugs

Mmp9 inhibitor I (444278) and Mmp9/13 inhibitor I (444252; Calbiochem/Millipore) were used at 100 µM. The EGFR inhibitor PD168393 (513033; Calbiochem/Millipore) was used at 10 µM. For all the experiments, drugs were added in embryo medium (5.0 mM NaCl, 0.17 mM KCl, 0.33 mM CaCl₂, and 0.33 mM MgSO₄) with 2% DMSO 6 h before the measurements or time-lapse started and remained present for the duration of the experiment.

Live imaging

For photos of live embryos at 30 hpf, the embryos were embedded in 2% methylcellulose (Sigma-Aldrich) in embryo medium with 0.04% tricaine (Sigma-Aldrich). For time-lapse vital microscopy, embryos

were embedded in 1% low-melting agar in embryo medium with 0.04% tricaine (Sigma-Aldrich). When imaging the periderm, recording started at 28 hpf and continued for 18 h, with images acquired at 8-min intervals. A 710 laser-scanning confocal (Zeiss) and spinning disk fluorescence (Nikon) microscopes were used. When imaging the basal layer, 2-h recordings were performed between 24 and 30 hpf with images collected at 2-min intervals. A 710 confocal fluorescence microscope (Zeiss) was used. Imaging was performed with a long working distance 20× lens. All the time-lapse studies were performed at 28.5°C. Image analysis was performed using Zeiss Black or Fiji ImageJ software.

Immunofluorescence staining and BrdU incorporation

For E-cadherin and p63 staining, embryos were fixed at 30 hpf in 4% PFA in PBS overnight and postfixed in methanol at −20°C overnight. Staining was performed as previously described (Reischauer et al., 2009). Mouse E-cadherin antibody (clone 36; 610181; BD Bioscience) was used at 1:100, rabbit p63 antibody (gtx124660; Genetex) at 1:100, and secondary antibodies conjugated with Alexa Fluor 564 and 647 (Life Technologies) at 1:500. For BrdU incorporation and staining, embryos at 28 hpf were incubated with 10 mM BrdU (Life Technologies) and 2% DMSO in embryo medium for 3 h followed by three 5-min washes in embryo medium. Embryos were then incubated for 15 h and fixed in PFA 4%. The BrdU staining was performed as described (Reischauer et al., 2009). Sheep BrdU antibody (ab1893; Abcam) was used at 1:100 and mouse p63 antibody (clone 4A4; sc8431; Santa Cruz Biotechnology) at 1:200. Immunostained embryos were imaged using a 710 confocal microscope and 20× and 40× long working distance lenses. Imaging analysis was performed using Zeiss Black or Fiji ImageJ software.

Keratinocyte isolation and quantitative PCR

Periderm and basal layer keratinocytes were sorted from Tg (*krt4 :nlsEGFP*)[cy34] and *TgBAC (ΔNp63:Gal4FF)*[la213]: *Tg (UAS:Lifeact -GFP)*[mu271] zebrafish embryos, respectively, as previously described (Manoli and Driever, 2012). In brief, 100 embryos of each genotype were manually dechorionated at 24 hpf. Cells were dispersed from embryos, and GFP-labeled cells were sorted using a FACS Aria2 (BD Bioscience) and lysed in Trizol (Sigma-Aldrich); RNA was purified using the RNeasy micro-kit (Qiagen) and converted to cDNA library using the SuperScript-Vilo kit (Life Technologies). Quantitative PCR was performed using TaqMan gene expression master mix (Life Technologies) according to the manufacturer's instructions. TaqMan-Fam Probes were ordered from Life Technologies. The reaction was performed with 7900HT Fast Real-Time PCR system (Applied Biosystems). Probes and assay IDs were as follows: reference gene *Eef1a1l*, assay ID: DR03432748_m1; *Il1b,* assay ID: DR03114367_g1; *Mmp2*, assay ID: DR03076189; *Mmp9*, assay ID: Dr03139883_g1; *Mmp13a*, assay ID: Dr03438514_g1; *St14a*, assay ID: AIS09DC; *Krt4*, assay ID: DR03093320_gh; *P63*, assay ID: Dr03131730_m1; *Spint1a*, assay ID: DR03139912_m1; and *F2rl1.2*, assay ID: Dr03168088.

Statistical analysis

One-way ANOVA with Bonferroni posttest or two-way ANOVA with Tukey posttest were used to identify significant differences between treatment groups. Sample sizes and p-values are indicated in figure legends. Asterisk in figures indicates significant differences after correction for multiple comparisons with p-value indicated in the legends. Calculations were done using Prism statistical software (GraphPad), and the level of statistical significance was set at $P < 0.05$ for initial ANOVA before any post-tests were permitted.

Online supplemental material

Fig. S1 shows photos of a mounted zebrafish embryo indicating the region selected for time-lapse imaging. Fig. S2 shows apical extrusion of cells from the trunk periderm cells in *hai1a* morphants. Fig. S3 shows distribution of nuclei and subcellular distribution of E-cadherin in periderm in control and *hai1a* morphants and effect of inhibition of mmp9/mmp13 (by drugs and MOs), erbb2 (by MO), and EGFR (by inhibitor PD168393). Fig. S4 shows leukocyte infiltration of skin in *hai1a* morphant and rescue by Par2b depletion. Video 1 show periderm in control with LifeAct-GFP marker. Video 2 shows periderm in *hai1a* morphant showing cell extrusion with LifeAct-GFP marker. Video 3 shows periderm in *hai1a* morphant showing multiple single cell extrusions from one site with LifeAct-GFP marker. Video 4 shows periderm in control using nuclear-GFP marker. Video 5 shows periderm in *hai1a* morphant showing clustering of extrusion events in an area of apparent cell crowding with nuclear-GFP marker. Video 6 shows periderm in *par2b* mutant/*hai1a* morphant showing increased nuclear division with nuclear-GFP marker. Video 7 shows rare extrusion of a periderm keratinocyte with nuclear fragmentation in a control embryo with nuclear-GFP marker. Video 8 shows a common event in *hai1a* morphants—extrusion of cells with an initially intact nucleus that appears to undergo nuclear envelope breakdown late in the process (with nuclear-GFP marker). Video 9 shows the basal layer in control showing stable cell–cell contact with LifeAct-GFP marker. Videos 10 and 11 show the basal layer in *hai1a* morphants showing lack of stable cell–cell interaction, filopodia and lamellipodia formation, and increased cell movement. with LifeAct-GFP marker Video 12 shows the basal layer in *hai1a* morphant showing swarming behavior with LifeAct-GFP marker. Video 13 shows basal layer in *st14a/hai1a* morphants showing restoration of stable cell–cell contact with LifeAct-GFP marker. Video 14 shows the basal layer in *par2a* mutant/*hai1a* morphant showing restoration of stable cell–cell contacts with LifeAct-GFP marker. Table S1 shows quantitative PCR data showing expression of mRNA for *hai1a*, *st14a*, and *par2b* in periderm and basal layer keratinocytes sorted from 24-hpf zebrafish embryos. *keratin4* and *tp63* are included as periderm and basal keratinocyte markers. Table S2 is a summary of effects of Par2b and St14a deficiency on Hai1a phenotypes. The supplemental data file shows nucleotide and predicted amino acid sequences of wild-type and TALEN mutant zebrafish *par2b*.

References

Antalis, T.M., T.H. Bugge, and Q. Wu. 2011. Membrane-anchored serine proteases in health and disease. *Prog. Mol. Biol. Transl. Sci.* 99:1–50. https://doi.org/10.1016/B978-0-12-385504-6.00001-4

Bocheva, G., A. Rattenholl, C. Kempkes, T. Goerge, C.Y. Lin, M.R. D'Andrea, S. Ständer, and M. Steinhoff. 2009. Role of matriptase and proteinase-activated receptor-2 in nonmelanoma skin cancer. *J. Invest. Dermatol.* 129:1816–1823. https://doi.org/10.1038/jid.2008.449

Buzza, M.S., S. Netzel-Arnett, T. Shea-Donohue, A. Zhao, C.Y. Lin, K. List, R. Szabo, A. Fasano, T.H. Bugge, and T.M. Antalis. 2010. Membrane-anchored serine protease matriptase regulates epithelial barrier formation and permeability in the intestine. *Proc. Natl. Acad. Sci. USA.* 107:4200–4205. https://doi.org/10.1073/pnas.0903923107

Buzza, M.S., E.W. Martin, K.H. Driesbaugh, A. Désilets, R. Leduc, and T.M. Antalis. 2013. Prostasin is required for matriptase activation in intestinal epithelial cells to regulate closure of the paracellular pathway. *J. Biol. Chem.* 288:10328–10337. https://doi.org/10.1074/jbc.M112.443432

Camerer, E., W. Huang, and S.R. Coughlin. 2000. Tissue factor- and factor X-dependent activation of protease-activated receptor 2 by factor VIIa. *Proc. Natl. Acad. Sci. USA.* 97:5255–5260. https://doi.org/10.1073/pnas.97.10.5255

Camerer, E., A. Barker, D.N. Duong, R. Ganesan, H. Kataoka, I. Cornelissen, M.R. Darragh, A. Hussain, Y.W. Zheng, Y. Srinivasan, et al. 2010. Local protease signaling contributes to neural tube closure in the mouse embryo. *Dev. Cell.* 18:25–38. https://doi.org/10.1016/j.devcel.2009.11.014

Carney, T.J., S. von der Hardt, C. Sonntag, A. Amsterdam, J. Topczewski, N. Hopkins, and M. Hammerschmidt. 2007. Inactivation of serine protease Matriptase1a by its inhibitor Hai1 is required for epithelial integrity of the zebrafish epidermis. *Development.* 134:3461–3471. https://doi.org/10.1242/dev.004556

Cermak, T., E.L. Doyle, M. Christian, L. Wang, Y. Zhang, C. Schmidt, J.A. Baller, N.V. Somia, A.J. Bogdanove, and D.F. Voytas. 2011. Efficient design and assembly of custom TALEN and other TAL effector-based constructs for DNA targeting. *Nucleic Acids Res.* 39:e82. https://doi.org/10.1093/nar/gkr218

Chen, C.F., C.Y. Chu, T.H. Chen, S.J. Lee, C.N. Shen, and C.D. Hsiao. 2011. Establishment of a transgenic zebrafish line for superficial skin ablation and functional validation of apoptosis modulators in vivo. *PLoS One.* 6:e20654. https://doi.org/10.1371/journal.pone.0020654

Cheng, M.F., M.S. Huang, C.S. Lin, L.H. Lin, H.S. Lee, J.C. Jiang, and K.T. Hsia. 2014. Expression of matriptase correlates with tumour progression and clinical prognosis in oral squamous cell carcinoma. *Histopathology.* 65:24–34. https://doi.org/10.1111/his.12361

Chung, H., R. Ramachandran, M.D. Hollenberg, and D.A. Muruve. 2013. Proteinase-activated receptor-2 transactivation of epidermal growth factor receptor and transforming growth factor-β receptor signaling pathways contributes to renal fibrosis. *J. Biol. Chem.* 288:37319–37331. https://doi.org/10.1074/jbc.M113.492793

Corvera, C.U., O. Déry, K. McConalogue, S.K. Böhm, L.M. Khitin, G.H. Caughey, D.G. Payan, and N.W. Bunnett. 1997. Mast cell tryptase regulates rat colonic myocytes through proteinase-activated receptor 2. *J. Clin. Invest.* 100:1383–1393. https://doi.org/10.1172/JCI119658

Coughlin, S.R. 2000. Thrombin signalling and protease-activated receptors. *Nature.* 407:258–264. https://doi.org/10.1038/35025229

Coughlin, S.R. 2005. Protease-activated receptors in hemostasis, thrombosis and vascular biology. *J. Thromb. Haemost.* 3:1800–1814. https://doi.org/10.1111/j.1538-7836.2005.01377.x

Darmoul, D., J.C. Marie, H. Devaud, V. Gratio, and M. Laburthe. 2001. Initiation of human colon cancer cell proliferation by trypsin acting at protease-activated receptor-2. *Br. J. Cancer.* 85:772–779. https://doi.org/10.1054/bjoc.2001.1976

Darmoul, D., V. Gratio, H. Devaud, and M. Laburthe. 2004. Protease-activated receptor 2 in colon cancer: Trypsin-induced MAPK phosphorylation and cell proliferation are mediated by epidermal growth factor receptor transactivation. *J. Biol. Chem.* 279:20927–20934. https://doi.org/10.1074/jbc.M401430200

Eisenhoffer, G.T., P.D. Loftus, M. Yoshigi, H. Otsuna, C.B. Chien, P.A. Morcos, and J. Rosenblatt. 2012. Crowding induces live cell extrusion to maintain homeostatic cell numbers in epithelia. *Nature.* 484:546–549. https://doi.org/10.1038/nature10999

Frateschi, S., E. Camerer, G. Crisante, S. Rieser, M. Membrez, R.P. Charles, F. Beermann, J.C. Stehle, B. Breiden, K. Sandhoff, et al. 2011. PAR2 absence completely rescues inflammation and ichthyosis caused by altered CAP1/Prss8 expression in mouse skin. *Nat. Commun.* 2:161. https://doi.org/10.1038/ncomms1162

Gu, Y., T. Forostyan, R. Sabbadini, and J. Rosenblatt. 2011. Epithelial cell extrusion requires the sphingosine-1-phosphate receptor 2 pathway. *J. Cell Biol.* 193:667–676. https://doi.org/10.1083/jcb.201010075

Gudipaty, S.A., and J. Rosenblatt. 2017. Epithelial cell extrusion: Pathways and pathologies. *Semin. Cell Dev. Biol.* 67:132–140. PubMed

Helker, C.S., A. Schuermann, T. Karpanen, D. Zeuschner, H.G. Belting, M. Affolter, S. Schulte-Merker, and W. Herzog. 2013. The zebrafish common cardinal veins develop by a novel mechanism: Lumen ensheathment. *Development.* 140:2776–2786. https://doi.org/10.1242/dev.091876

Hirota, Y., Y. Osuga, T. Hirata, M. Harada, C. Morimoto, O. Yoshino, K. Koga, T. Yano, O. Tsutsumi, and Y. Taketani. 2005. Activation of protease-activated receptor 2 stimulates proliferation and interleukin (IL)-6 and IL-8 secretion of endometriotic stromal cells. *Hum. Reprod.* 20:3547–3553. https://doi.org/10.1093/humrep/dei255

Hu, L., L. Xia, H. Zhou, B. Wu, Y. Mu, Y. Wu, and J. Yan. 2013. TF/FVIIa/PAR2 promotes cell proliferation and migration via PKCα and ERK-dependent c-Jun/AP-1 pathway in colon cancer cell line SW620. *Tumour Biol.* 34:2573–2581. https://doi.org/10.1007/s13277-013-0803-2

Kiener, T.K., I. Selptsova-Friedrich, and W. Hunziker. 2008. Tjp3/zo-3 is critical for epidermal barrier function in zebrafish embryos. *Dev. Biol.* 316:36–49. https://doi.org/10.1016/j.ydbio.2007.12.047

Kwong, R.W., and S.F. Perry. 2013. The tight junction protein claudin-b regulates epithelial permeability and sodium handling in larval zebrafish, Danio rerio. *Am. J. Physiol. Regul. Integr. Comp. Physiol.* 304:R504–R513. https://doi.org/10.1152/ajpregu.00385.2012

LeBert, D.C., J.M. Squirrell, J. Rindy, E. Broadbridge, Y. Lui, A. Zakrzewska, K.W. Eliceiri, A.H. Meijer, and A. Huttenlocher. 2015. Matrix metalloproteinase 9 modulates collagen matrices and wound repair. *Development.* 142:2136–2146. https://doi.org/10.1242/dev.121160

Le Gall, S.M., R. Szabo, M. Lee, D. Kirchhofer, C.S. Craik, T.H. Bugge, and E. Camerer. 2016. Matriptase activation connects tissue factor-dependent coagulation initiation to epithelial proteolysis and signaling. *Blood.* 127:3260–3269. https://doi.org/10.1182/blood-2015-11-683110

Le Guellec, D., G. Morvan-Dubois, and J.Y. Sire. 2004. Skin development in bony fish with particular emphasis on collagen deposition in the dermis of the zebrafish (Danio rerio). *Int. J. Dev. Biol.* 48:217–231. https://doi.org/10.1387/ijdb.15272388

List, K., C.C. Haudenschild, R. Szabo, W. Chen, S.M. Wahl, W. Swaim, L.H. Engelholm, N. Behrendt, and T.H. Bugge. 2002. Matriptase/MT-SP1 is required for postnatal survival, epidermal barrier function, hair follicle development, and thymic homeostasis. *Oncogene.* 21:3765–3779. https://doi.org/10.1038/sj.onc.1205502

List, K., P. Kosa, R. Szabo, A.L. Bey, C.B. Wang, A. Molinolo, and T.H. Bugge. 2009. Epithelial integrity is maintained by a matriptase-dependent proteolytic pathway. *Am. J. Pathol.* 175:1453–1463. https://doi.org/10.2353/ajpath.2009.090240

Ludeman, M.J., Y.W. Zheng, K. Ishii, and S.R. Coughlin. 2004. Regulated shedding of PAR1 N-terminal exodomain from endothelial cells. *J. Biol. Chem.* 279:18592–18599.

Lyons, D.A., H.M. Pogoda, M.G. Voas, I.G. Woods, B. Diamond, R. Nix, N. Arana, J. Jacobs, and W.S. Talbot. 2005. erbb3 and erbb2 are essential for Schwann cell migration and myelination in zebrafish. *Curr. Biol.* 15:513–524. https://doi.org/10.1016/j.cub.2005.02.030

Manoli, M., and W. Driever. 2012. Fluorescence-activated cell sorting (FACS) of fluorescently tagged cells from zebrafish larvae for RNA isolation. *Cold Spring Harb. Protoc.* 2012:prot069333. https://doi.org/10.1101/pdb.prot069633

Marchiando, A.M., W.V. Graham, and J.R. Turner. 2010. Epithelial barriers in homeostasis and disease. *Annu. Rev. Pathol.* 5:119–144. https://doi.org/10.1146/annurev.pathol.4.110807.092135

Mathias, J.R., B.J. Perrin, T.X. Liu, J. Kanki, A.T. Look, and A. Huttenlocher. 2006. Resolution of inflammation by retrograde chemotaxis of neutrophils in transgenic zebrafish. *J. Leukoc. Biol.* 80:1281–1288. https://doi.org/10.1189/jlb.0506346

Mathias, J.R., M.E. Dodd, K.B. Walters, J. Rhodes, J.P. Kanki, A.T. Look, and A. Huttenlocher. 2007. Live imaging of chronic inflammation caused by mutation of zebrafish Hai1. *J. Cell Sci.* 120:3372–3383. https://doi.org/10.1242/jcs.009159

Michel, N., N. Heuzé-Vourc'h, E. Lavergne, C. Parent, M.L. Jourdan, A. Vallet, S. Iochmann, O. Musso, P. Reverdiau, and Y. Courty. 2014. Growth and survival of lung cancer cells: Regulation by kallikrein-related peptidase 6 via activation of proteinase-activated receptor 2 and the epidermal growth factor receptor. *Biol. Chem.* 395:1015–1025. https://doi.org/10.1515/hsz-2014-0124

Nonboe, A.W., O. Krigslund, C. Soendergaard, S. Skovbjerg, S. Friis, M.N. Andersen, V. Ellis, M. Kawaguchi, H. Kataoka, T.H. Bugge, and L.K. Vogel. 2017. HAI-2 stabilizes, inhibits and regulates SEA-cleavage-dependent secretory transport of matriptase. *Traffic.* 18:378–391. https://doi.org/10.1111/tra.12482

Nystedt, S., K. Emilsson, C. Wahlestedt, and J. Sundelin. 1994. Molecular cloning of a potential proteinase activated receptor. *Proc. Natl. Acad. Sci. USA.* 91:9208–9212. https://doi.org/10.1073/pnas.91.20.9208

Oberst, M.D., L.Y. Chen, K. Kiyomiya, C.A. Williams, M.S. Lee, M.D. Johnson, R.B. Dickson, and C.Y. Lin. 2005. HAI-1 regulates activation and expression of matriptase, a membrane-bound serine protease. *Am. J. Physiol. Cell Physiol.* 289:C462–C470. https://doi.org/10.1152/ajpcell.00076.2005

Page-McCaw, A., A.J. Ewald, and Z. Werb. 2007. Matrix metalloproteinases and the regulation of tissue remodelling. *Nat. Rev. Mol. Cell Biol.* 8:221–233. https://doi.org/10.1038/nrm2125

Ragkousi, K., and M.C. Gibson. 2014. Cell division and the maintenance of epithelial order. *J. Cell Biol.* 207:181–188. https://doi.org/10.1083/jcb.201408044

Rasmussen, J.P., G.S. Sack, S.M. Martin, and A. Sagasti. 2015. Vertebrate epidermal cells are broad-specificity phagocytes that clear sensory axon debris. *J. Neurosci.* 35:559–570. https://doi.org/10.1523/JNEUROSCI.3613-14.2015

Rattenholl, A., S. Seeliger, J. Buddenkotte, M. Schon, M.P. Schon, S. Stander, N. Vergnolle, and M. Steinhoff. 2007. Proteinase-activated receptor-2 (PAR2): A tumor suppressor in skin carcinogenesis. *J. Invest. Dermatol.* 127:2245–2252.

Reischauer, S., M.P. Levesque, C. Nüsslein-Volhard, and M. Sonawane. 2009. Lgl2 executes its function as a tumor suppressor by regulating ErbB signaling in the zebrafish epidermis. *PLoS Genet.* 5:e1000720. https://doi.org/10.1371/journal.pgen.1000720

Sales, K.U., S. Friis, L. Abusleme, N.M. Moutsopoulos, and T.H. Bugge. 2015a. Matriptase promotes inflammatory cell accumulation and progression of established epidermal tumors. *Oncogene.* 34:4664–4672. https://doi.org/10.1038/onc.2014.391

Sales, K.U., S. Friis, J.E. Konkel, S. Godiksen, M. Hatakeyama, K.K. Hansen, S.R. Rogatto, R. Szabo, L.K. Vogel, W. Chen, et al. 2015b. Non-hematopoietic PAR-2 is essential for matriptase-driven pre-malignant progression and potentiation of ras-mediated squamous cell carcinogenesis. *Oncogene.* 34:346–356. https://doi.org/10.1038/onc.2013.563

Shi, K., K.C. Queiroz, J. Stap, D.J. Richel, and C.A. Spek. 2013. Protease-activated receptor-2 induces migration of pancreatic cancer cells in an extracellular ATP-dependent manner. *J. Thromb. Haemost.* 11:1892–1902.

Simpson, C.L., D.M. Patel, and K.J. Green. 2011. Deconstructing the skin: Cytoarchitectural determinants of epidermal morphogenesis. *Nat. Rev. Mol. Cell Biol.* 12:565–580. https://doi.org/10.1038/nrm3175

Slanchev, K., T.J. Carney, M.P. Stemmler, B. Koschorz, A. Amsterdam, H. Schwarz, and M. Hammerschmidt. 2009. The epithelial cell adhesion molecule EpCAM is required for epithelial morphogenesis and integrity during zebrafish epiboly and skin development. *PLoS Genet.* 5:e1000563. https://doi.org/10.1371/journal.pgen.1000563

Sonawane, M., H. Martin-Maischein, H. Schwarz, and C. Nüsslein-Volhard. 2009. Lgl2 and E-cadherin act antagonistically to regulate hemidesmosome

formation during epidermal development in zebrafish. *Development.* 136:1231–1240. https://doi.org/10.1242/dev.032508

Steinhoff, M., U. Neisius, A. Ikoma, M. Fartasch, G. Heyer, P.S. Skov, T.A. Luger, and M. Schmelz. 2003. Proteinase-activated receptor-2 mediates itch: A novel pathway for pruritus in human skin. *J. Neurosci.* 23:6176–6180.

Szabo, R., and T.H. Bugge. 2011. Membrane-anchored serine proteases in vertebrate cell and developmental biology. *Annu. Rev. Cell Dev. Biol.* 27:213–235. https://doi.org/10.1146/annurev-cellbio-092910-154247

Szabo, R., J.P. Hobson, K. Christoph, P. Kosa, K. List, and T.H. Bugge. 2009. Regulation of cell surface protease matriptase by HAI2 is essential for placental development, neural tube closure and embryonic survival in mice. *Development.* 136:2653–2663. https://doi.org/10.1242/dev.038430

Szabo, R., D.E. Peters, P. Kosa, E. Camerer, and T.H. Bugge. 2014. Regulation of feto-maternal barrier by matriptase- and PAR-2-mediated signaling is required for placental morphogenesis and mouse embryonic survival. *PLoS Genet.* 10:e1004470. https://doi.org/10.1371/journal.pgen.1004470

Takeuchi, T., J.L. Harris, W. Huang, K.W. Yan, S.R. Coughlin, and C.S. Craik. 2000. Cellular localization of membrane-type serine protease 1 and identification of protease-activated receptor-2 and single-chain urokinase-type plasminogen activator as substrates. *J. Biol. Chem.* 275:26333–26342. https://doi.org/10.1074/jbc.M002941200

Volkmann, K., Y.Y. Chen, M.P. Harris, M.F. Wullimann, and R.W. Köster. 2010. The zebrafish cerebellar upper rhombic lip generates tegmental hindbrain nuclei by long-distance migration in an evolutionary conserved manner. *J. Comp. Neurol.* 518:2794–2817.

Vu, T.K., D.T. Hung, V.I. Wheaton, and S.R. Coughlin. 1991a. Molecular cloning of a functional thrombin receptor reveals a novel proteolytic mechanism of receptor activation. *Cell.* 64:1057–1068. https://doi.org/10.1016/0092-8674(91)90261-V

Vu, T.K., V.I. Wheaton, D.T. Hung, I. Charo, and S.R. Coughlin. 1991b. Domains specifying thrombin-receptor interaction. *Nature.* 353:674–677. https://doi.org/10.1038/353674a0

Wang, Z. 2016. Transactivation of epidermal growth factor receptor by G protein-coupled receptors: Recent progress, challenges and future research. *Int. J. Mol. Sci.* 17:E95.

Winter, M.C., S.S. Shasby, D.R. Ries, and D.M. Shasby. 2006. PAR2 activation interrupts E-cadherin adhesion and compromises the airway epithelial barrier: Protective effect of beta-agonists. *Am. J. Physiol. Lung Cell. Mol. Physiol.* 291:L628–L635. https://doi.org/10.1152/ajplung.00046.2006

Wu, C.J., X. Feng, M. Lu, S. Morimura, and M.C. Udey. 2017. Matriptase-mediated cleavage of EpCAM destabilizes claudins and dysregulates intestinal epithelial homeostasis. *J. Clin. Invest.* 127:623–634. https://doi.org/10.1172/JCI88428

Xu, H., N. Echemendia, S. Chen, and F. Lin. 2011. Identification and expression patterns of members of the protease-activated receptor (PAR) gene family during zebrafish development. *Dev. Dyn.* 240:278–287. https://doi.org/10.1002/dvdy.22517

Yau, M.K., L. Liu, and D.P. Fairlie. 2013. Toward drugs for protease-activated receptor 2 (PAR2). *J. Med. Chem.* 56:7477–7497. https://doi.org/10.1021/jm400638v

Zhao, P., M. Metcalf, and N.W. Bunnett. 2014. Biased signaling of protease-activated receptors. *Front. Endocrinol. (Lausanne).* 5:67.